

Development and validation of an efficient direct numerical optimisation approach for aerofoil shape design

M. Khurana and H. Winarto

manas.khurana@rmit.edu.au

The Sir Lawrence Wackett Aerospace Centre

RMIT University

Melbourne

Australia

ABSTRACT

Intelligent shape optimisation architecture is developed, validated and applied in the design of high-altitude long endurance aerofoil (HALE). The direct numeric optimisation (DNO) approach integrating a geometrical shape parameterisation model coupled to a validated flow solver and a population based search algorithm are applied in the design process. The merit of the DNO methodology is measured by computational time efficiency and feasibility of the optimal solution. Gradient based optimisers are not suitable for multimodal solution topologies. Thus, a novel particle swarm optimiser with adaptive mutation (AM-PSO) is developed. The effect of applying the PARSEC and a modified variant of the original function, as a shape parameterisation model on the global optimal is verified. Optimisation efficiency is addressed by mapping the solution topology for HALE aerofoil designs and by computing the sensitivity of aerofoil shape variables on the objective function. Variables with minimal influence are identified and eliminated from shape optimisation simulations. Variable elimination has a negligible effect on the aerodynamics of the global optima, with a significant reduction in design iterations to convergence. A novel data-mining technique is further applied to verify the accuracy of the AM-PSO solutions. The post-processing analysis, to swarm optimisation solutions, indicates a hybrid optimisation methodology with the integration of global and local gradient based search methods, yields a true optima. The findings are consistent for single and multi-point designs.

NOMENCLATURE

c	aerofoil chord length
c_1	cognitive coefficient
c_2	social coefficient
c_d	coefficient of drag
c_j	constraint cost repair constant
c_l	coefficient of lift
c_l^T	target lift coefficient
c_{lmax}	maximum coefficient of lift
c_m	coefficient of moment
c_p	coefficient of pressure
c_{m0}	coefficient of moment at zero lift
c_p^T	target coefficient of pressure
D	problem dimension
$d_i(x)$	elementary effect of input vector
d_j	constraint function distance metric
f_p	penalised fitness
K	constriction factor
k	number of design variables
M	aerofoil chord partition size
M_∞	freestream Mach number
n	number of particles in the swarm
p_j	personal best fitness range of the swarm
$pbest_i^p$	best personal solution of the particle
$pbestg$	best global solution of swarm

r_1 & r_2	randomly generated numbers (0,1)
R_n	Reynolds number
t	Iteration
t/c	aerofoil thickness-to-chord
v_i	velocity vector in dimension D
x	vector of design variables
x/c	aerofoil chord
x_i	position vector in dimension D
y	output of objective function for sensitivity analysis
$(y/c)_{approx}$	approximate aerofoil shape
$(y/c)_{target}$	target aerofoil shape
α	angle-of-attack
α_{max}	angle-of-attack for maximum lift
β	aerofoil trailing edge angle
Δ	elementary effect step length factor
η_{con}	number of constraints
$\frac{dc_p}{dx}$	adverse pressure gradient
\mathfrak{J}	objective function
μ^*	absolute mean of elementary effect
μ_M and σ_M	mean and standard deviation of elementary effect
ω	objective weighting magnitude
ω_i	standard deviation of personal best solution
Φ_{op}	aerofoil operating conditions
σ_i	standard deviation of the swarm
φ	search tolerance factor

Abbreviations

AM-PSO	adaptive-mutated particle swarm optimiser
DNO	direct numeric optimisation
GA	genetic algorithm
GM	gradient-based optimiser method
HALE	high-altitude long endurance
HRN	high Reynolds number ($Rn > 9.0 \times 10^6$)
LRN	low Reynolds number ($Rn \approx 0.15 \times 10^6$)
LSB	laminar separation bubble
MRN	medium Reynolds number ($Rn \approx 4.0 \times 10^6$)
PSO	particle swarm optimiser
RANS	Reynolds averaged Navier Stokes
SOM	self-organising map

1.0 INTRODUCTION

The process of shape optimisation is critical for development of efficient aerial platforms to meet the stipulated aerodynamic performance requirements. This requires a multi-disciplinary design optimisation process, for the performance requirements in various phases of flight profile. The planform is to be aerodynamically efficient and structurally viable for flight maneuver loads. Wing contour is governed by aerofoils at each span station. The acceptable drag performance of the aerofoil is a function of Mach number, operating cruise altitude and hence, Reynolds number and lift requirements. The design parameters that influence aerofoil performance are leading edge radius, camber, thickness-to-chord ratio and trailing edge wedge angle between aerofoil upper and lower surfaces. A shape optimisation analysis is required to establish an aerofoil profile with acceptable aerodynamic performance. This research focuses on developing intelligent algorithms for aerofoil shape optimisation for a UAVs operating in a HALE environment.

1.1 Inverse design

Aerofoil design efforts include the 'inverse' and 'direct' methods. The inverse approach requires the specification of a velocity profile for the required mission requirements. Long endurance

flights require extended regions of laminar flow to minimise c_{d0} . The requirement is established by specifying a velocity/pressure distribution profile, that extends the favorable pressure gradient downstream of the leading edge radius, to a specified aerofoil chord station x/c . The objective function is defined by a least square formulation, where the target pressure distribution c_p^T , must match the computed c_p , along aerofoil chord x/c , at point i , over M partitions:

$$\mathfrak{J} \min = \sum_{i=1}^M |c_p(x/c_i) - c_p^T(x/c_i)| \quad \dots (1)$$

The demerit of this approach is transforming the mission requirements to a velocity profile. The transformation of the desired boundary-layer characteristics into a pressure distribution is left to the imagination of the aerofoil designer⁽¹⁾. Establishment of valid velocity profile does not guarantee an aerodynamically feasible shape. The generation of a 'fish-tail' aerofoil with the upper and lower surfaces bisecting, is a possible solution. Thus, the input velocity profile will require re-adjustment to address the issue. Hence, the inverse approach is not considered in this paper.

1.2 Direct design

The use of a direct method is an alternate to the inverse approach for shape design. The methodology requires the integration of a geometry shape parameterisation model to represent an arbitrary aerofoil/wing, to a flow solver for aerodynamic analysis and an optimisation algorithm for an intelligent search analysis. The components operate in iteration for convergence based on defined objectives and constraints. The objective function defined minimises the drag coefficient c_d , at cruise, by maintaining the target lift coefficient c_l^T subject to a geometrical constraint of thickness-to-chord t/c , bounded by a lower and upper limit t/c^L and t/c^U respectively. This is presented in Equation (2).

$$\begin{aligned} J_{min} &= c_d \\ \text{subject to: } &c_l \geq c_l^T \\ &: t/c^L < t/c < t/c^U \end{aligned} \quad \dots (2)$$

1.3 Background and literature survey

The DNO methodology comprises of three components: a) Aerofoil shape parameterisation model; b) Validated flow solver; and c) Optimisation algorithm. The components operate in iteration to generate an optimal shape based on defined objectives and constraints. Hence, the components are validated to ensure a feasible solution as an output to the optimisation process. Aerofoil shape parameterisation model defines the search space to the optimisation problem. Aerodynamic solvers capture flow features from shock development for transonic flows to laminar separation bubbles at low-speeds. The limitation of the computational code must be identified. The optimisation process is governed by the search algorithm applied. The optimiser is developed and tuned for a valid search process and is problem dependent. This section investigates numerical techniques used in the DNO approach.

The earliest reported aerodynamic shape optimisation analysis, originated in wing design by Hicks *et al*⁽²⁾. Hicks integrated a fully potential, inviscid aerodynamics code, coupled with a conjugate gradient optimisation algorithm, based on the steepest descent direction of the objective function⁽²⁾. Shape parameterisation was achieved by adding a series of sinusoidal curves (Hicks-Henne functions), to a baseline shape to generate a new geometry.

Hicks supports the direct approach over the inverse method, as off-design conditions are automatically considered during the optimisation process⁽²⁾. The study reported several recommendations for numerical design techniques⁽²⁾, including increased computational

resources. It was concluded that a detail mesh study is required, with minimal number of grid points, without compromising aerodynamic data for efficient optimisation. The convergence criteria needs close analysis to enhance the search process. The final recommended conclusion was based on the development of a flexible shape representation model⁽²⁾. A limited geometry model does not confirm a global optimal solution, thus the search capabilities of the optimiser is limited by the deficiency of the shape model.

Research efforts for robust and efficient DNO structure development are based on the recommendations of Hicks *et al.*⁽²⁾. A survey of DNO components covers: a) aerofoil shape parameterisation; b) validated flow solver; and c) intelligent search optimisation algorithm.

1.3.1 Aerofoil shape parameterisation

Aerofoil shape representation strategies for optimisation include: a) Knowledge-Based; and b) Free-Form. In the knowledge-based design, an algebraic expression is applied to represent a series of sinusoidal curves, which are multipliers to the design coefficients to represent disparate aerofoil shapes. In the freeform methodology, the shape is represented by a linear combination of basis functions including splines.

The discrete approach is an obvious candidate for aerofoil representation. The method is quick and easy to implement, with wall surface boundary nodes used as design variables. Theoretically, the methodology will generate infinite aerofoil classes. Thus, the issue of a reduced solution search space, due to a limited geometry model is avoided. Despite an enhanced search space, the methodology is unsuitable for numerical optimisation. With each node regarded as a design variable, the combinatorial-permutation during search optimisation will be excessive, thus result in an inefficient search process. The optimiser further requires the generation of random solution for search initialisation. Randomly varying a large node population can result in the generation of an ill-defined shape with rapid surface concavities and abrupt changes in curvature as reported by Keane and Nair⁽³⁾.

Polynomial and spline curve interpolation methods for aerofoil shape representation are used to address the demerit of the discrete approach for shape optimisation⁽⁴⁻⁸⁾. The shape nodes are partitioned along aerofoil chord to control camber and thickness distributions. A large population of control points, in excess of twenty are required to generate smooth shapes. Since the chord station of the control nodes is fixed and the degree-of-freedom restricted to y -axis, generation of undulating shapes which are aerodynamically unfeasible becomes a design issue. Thus, even with a large population of control points for design flexibility, generation of unrealistic shapes is possible.

The PARSEC aerofoil shape representation model by Sobieczky⁽⁹⁾, is a sixth-order polynomial function applied to generate disparate aerofoil classes and is similar to the NACA 4-digit generator. The methodology is characterised by eleven design coefficients which control important aerofoil shape parameters including: a) Leading edge radius; b) Curvature of the upper and lower crests; c) Ordinates and abscissa of the upper and lower surfaces; d) Trailing edge ordinate thickness and location; and e) Trailing edge wedge angle. Variants of the original method have been developed to model divergent trailing edge aerofoils, to further increase the design flexibility of the shape function. Since the parameterisation method provides direct control over important aerofoil shape features, it is ideal for preliminary optimisation analysis. The method has been used in the design optimisation of transonic aerofoils, thick aerofoils for HALE operations and for low Reynolds number operations. The process of generating aerofoil contours, in the design of HALE aerofoils is modified in this paper, to further increase the design flexibility of the model.

1.3.2 Flow solver

The fitness of the objective function for aerodynamic shape optimisation is calculated from the flow solver. The output must be of consistent accuracy for an acceptable optimisation. Solver types include: a) Fully potential; b) Coupled boundary-layer; c) Euler; and d) Viscous Navier-Stokes. The merits and demerits must be considered for integration into optimisation architecture.

At HALE operations, viscous/inviscid interactions are critical at low Reynolds numbers. Navier-Stokes solvers are applied as it considers the viscous effects in the entire flow region and solves the Reynolds Average Navier-Stokes (RANS) equations of the flow. In laminar flow, a Laminar Separation Bubble (LSB), due to adverse pressure gradients in the boundary layer are formed at low lift coefficients. Sophisticated RANS with turbulence modeling are applied and validated to solve complicated flow patterns, including the LSB developed⁽¹⁰⁻¹¹⁾.

1.3.3 Optimisation algorithms

The choice of optimisation architecture will influence simulation run time and solution optimality. The two main optimiser types are: a) gradient-based and; b) evolutionary algorithms. Aerodynamic shape optimisation requires the stipulation of geometry and aerodynamic constraints. The constraints are often nonlinear and the optimiser solves the design limits to establish the minimum of a nonlinear objective function. Thus, the search topology will consist of multiple local minima and a robust search process becomes a requirement. The merits and demerits of the optimiser type proposed must be considered.

Gradient-based methods

Gradient-based methods (GM), have been widely used for aerodynamic shape optimisation problems. The algorithm perturbs the design variables, to minimise the objective function iteratively by modifying the direction of the gradient vector toward a solution.

The use of GM is problem dependent. If the objective function and constraints are continuous and differentiable and provide a unimodal convex domain, then GM is ideal. It has been shown that aerodynamic optimisation problems are non-smooth or non-convex^(15,16) thus, the use of GM will have issues and challenges. Generally GM, with an ill-defined starting point, will generate a local optimum in the neighborhood of the search initialisation point. The application of constraints further complicates the search process. Sequential quadratic programming methods were developed to handle objective constraints. Equality and inequality constraints are handled in the same manner as objectives (i.e. reduced for minimisation functions). Hence, the Jacobian matrix is calculated for both the constraints and the objectives. If the objective function can no longer be improved, without deteriorating the constraint values, the search will stagnate and prematurely terminate.

Namgoong⁽¹⁵⁾ examined the use of GM in the design optimisation of transonic aerofoils with variations in solution starting point, for wave drag minimisation. The results indicated disparate solutions with respect to initial base aerofoils, thus indicating a highly multimodal design space with numerous local minima. Gallarat⁽⁴⁾ evaluates the performance of three GM tools in the design optimisation of an aerofoil for morphing aircraft. It is acknowledged that the proposed method does not guarantee a global optimum. Khurana *et al.*⁽¹⁷⁾ established the solution space to HALE aerofoil designs, to be highly multimodal. Despite integrating a current off-the-shelf HALE aerofoil for search initialisation, aerodynamic performance improvement in comparison to the baseline shape was minimal⁽¹⁷⁾. It was concluded that GM provides a local solution about the starting point and not the true global optima⁽¹⁷⁾. Thus, the development of a global search operator is a requirement.

Adjoint methods

Post Hicks and Henne, advancements in gradient methods by the adjoint formulation have been applied for shape optimisation. The gradient is formulated by solving a set of adjoint partial differential equations, instead of evaluating the derivatives using finite differencing. The gradient of the objective function is related to the state (flow) equations. Thus, the computational time does not depend on the number of design variables, but is limited to the resources required to solve the flow equations. The method has drawbacks which must be considered. Premature convergence to local minima is an issue, hence a well-defined starting point is a requirement. Additionally, the method requires the derivation of an entirely new system of partial differential equations in terms of non-physical adjoint variables and the specification of the equating boundary conditions⁽¹⁵⁾. It has also been proven that the accuracy of the continuous adjoint method depends on the discretisation scheme, which must be as close as possible to that used for discretisation of the state equations⁽¹⁸⁾.

Evolutionary algorithms – Global search methods

Evolutionary algorithms (EA) also referred to as global search methods and are developed to mimic the process of natural evolution. Theoretically, EAs have the advantage of yielding a global optima by overcoming the limitations of the deterministic gradient-based search methods. Candidate solutions to the optimisation problem are characterised by a set of search agents or sample population, which evolve in the search environment, to achieve an acceptable solution to the objective function. The method is computationally demanding in comparison to local methods, as individual search agents must be evaluated by the fitness function. For CFD applications this leads to a time consuming search process and the use of parallel processing becomes a requirement.

The methodology is ideal for multimodal and discontinuous search topologies. An assumption of a smooth and continuous search space is not necessary, unlike local search processes. Global methods are not guided by the differential landscape. Constraint violations are handled with penalty functions, which are aggregates of the constraint violation magnitude. These are added to the objective function to penalise the search operator and to further guide the search away from ill-constraint solution topologies. Premature convergence as a result of constraint violation of a search agent is not an issue with global methods, since the search patterns of the entire population is assessed, to measure the termination criterion. Comparably, GM methods converge prematurely hence are not accurate for highly constrained aerodynamic shape optimisation problems.

Global methods are applicable over disparate problem types. Widely used methods include genetic algorithms (GA)⁽¹⁹⁾, simulated annealing (SA)⁽²⁰⁾, and ant colony (AC)⁽²¹⁾. The search methods are effective for design optimisations, but are computationally intensive due to the implementation of time-exhaustive search operators such as crossovers and mutations.

An alternate heuristic methodology inspired from the notion of ‘collective intelligence’ in biological populations, is the Particle Swarm Optimiser (PSO), by Kennedy *et al*⁽²²⁾. The method is developed to address the demerits of a time-exhaustive search process of the GA methods by avoiding the use of reproductive population generators by crossovers and mutation. Test simulation comparisons over disparate problems have shown that PSO exhibits accelerated convergence to the global solution in comparison to GA.

1.4 Scope

The design development and validation of a DNO architecture applied for HALE aerofoil shape design has not been covered in detail. Thus, the feasibility of the final solution cannot be assessed with confidence. The sub-components of the DNO structure are problem based and must be defined for HALE aerofoil shape design.

The paper is structured as follows:

Sec. 2.0: The sub-components of the DNO structure are defined and the desirable features for an effective search model addressed;

Sec. 3.0: A novel variant to the original PSO algorithm is proposed. A test development and validation analysis over benchmark test functions is presented. Performance results are compared against theoretical solutions to the test functions and against published data from the literature;

Sec. 4.0: The solution space for HALE aerofoil design is defined. An inverse shape fitting optimisation study is formulated to determine the search bounds of the design variables. The dimensionality of the problem is examined by a sensitivity analysis, to determine the importance of each aerofoil variable on HALE aerofoil aerodynamics;

Sec. 5.0: Aerofoil shape optimisation at single and multi-point designs is simulated with the developed optimisation architecture. A post-processing analysis is presented to verify the feasibility / optimality of the final solution; and

Sec. 6.0: The research findings are summarised and a statement on future related works is defined.

2.0 PROBLEM DEFINITION

The development of a valid DNO architecture for shape optimisation is dependent on the set-up of the DNO sub-components. The DNO modules of shape parameterisation, flow solver and optimisation algorithm require user-defined inputs. These must be well-defined through a design and validation study, so that the feasibility of the optimal shape can be analysed with confidence.

2.1 Aerofoil shape parameterisation

Several techniques exist for aerofoil representation (Section 1.3.1). The key properties that must be addressed include:

- generate smooth and realistic shapes;
- mathematically efficient so that shapes are generated with negligible computational effort;
- minimal design variable population while satisfying an acceptable design solution space;
- provide direct control over aerofoil thickness-to-chord, camber, leading edge radius, trailing-edge wedge angles and trailing edge direction;
- provide ease of control for aerofoil curve editing / modifications for a given optimal shape; and
- the design variables must be intuitive to geometric interpretation, so that optimisation process is guided by the shape variables to a feasible solution.

The PARSEC shape method addresses these requirements. The PARSEC-Original method generates profiles with upper and lower surfaces coupled during the shape parameterisation process. Due to the coupling effects, generation of highly-cambered nose aerofoils becomes a design issue thus, affecting design flexibility. The demerit of the original version is addressed by a modified version denoted by the PARSEC-modified approach. In this methodology, shape generation is decoupled with upper and lower aerofoil contours parameterised independently. The demerit is the introduction of three additional design variables, which adds complexity to search topology. The performance of the two PARSEC variants for HALE shape designs is assessed.

Aerofoil shape parameters must be controlled intelligently during the optimisation process to avoid unwanted flow features. Thus, the search algorithm determines a valid combinatorial-permutation set of design variables, that provide an acceptable solution to the problem. The leading edge radius must be controlled to avoid sudden changes in curvature at the joins of the nose region. Hence, early flow separation is avoided. Upper and lower crest curvatures at the maximum surface thickness point, must be controlled to avoid early transition to premature separation, which will have an unfavorable effect on drag. The optimisation algorithm will dynamically modify the shape variables through an intelligent and iterative search process, to minimise the unwanted flow features, as a result of shape modification.

2.2 Flow solver

Navier-Stokes simulations are required to model the viscous effects in separated flow. The aerofoil shape optimisation problem considered is at cruise thus, attached flow is assumed. Hence, panel methods are applied and calculate the effects of viscosity due to the development of a boundary layer, at low Reynolds numbers with acceptable accuracy. For attached flow, XFOIL provides acceptable agreement to published experimental data. The solver is prone to errors if surface geometry node distribution is not adequate. A convergence study was defined to determine the influence of node population, on the aerodynamic forces and the resulting errors. Empirical experiments were formulated and it was concluded that a population of 160 points, on aerofoil surface is required for acceptable aerodynamic convergence. Differences between computational and experimental data level-off at this point. Hence, a further increase in node population has a negligible effect on the aerodynamic forces. The calculated panel distribution is further recommended by the developers for computation at HALE conditions⁽²³⁾.

The aim of the presented analysis is to validate the proposed shape optimisation model. Panel methods are ideal for preliminary design developments, due to rapid computational turnover hence, the robustness of the proposed search algorithm can be assessed efficiently. Since 2-dimensional shapes with attached flow are examined, XFOIL is applied and provides acceptable accuracy with negligible computing resources. The solver is well suited for optimisation algorithm design application and validation.

2.3 Optimisation algorithm

The optimiser type significantly affects the search capabilities and the validity of the final solution. If the algorithm is limited, then a sub-optimal solution is probable. The following points must be taken into consideration when applying a search agent for aerofoil shape optimisation:

- number of design variables: Large population of variables result in an computationally time excessive optimisation run, especially if high-fidelity flow solvers are used;
- dynamic range of each dimension/variable: This equates to the search region that will be mapped by the optimiser;
- impose design variable constraints: Avoid mapping regions that result in ill-poised solutions;
- optimisation model: Provide global search behavior with the flexibility to parallelise the search process through distributed computing cluster; and
- validation: Evaluate the robustness of the selected optimisation model. Benchmark mathematical functions, where the global solution is known, can be used to test the robustness of the optimiser.

3.0 PARTICLE SWARM OPTIMISER

The PSO methodology is based on the evolution of nature to emulate a swarm behavior of insects, to a flock of birds or school of fish, which operate collaboratively to position food sources in the most efficient manner. In PSO, each search member is referred to as the particle, which represents a candidate solution to the problem.

Consider an i^{th} member of the population, represented by its position as $x_i^D = (x_i^1, x_i^2, \dots, x_i^D)$ and velocity $v_i^D = (v_i^1, v_i^2, \dots, v_i^D)$ in the solution search space. Unlike GM, a PSO does not require the gradient information of the objective function to establish the search direction. The method is easily facilitated in standard programming language using only primitive mathematical operators. The method also does not require an initial starting point with the initial swarm randomly generated, followed by an iterative search process which updates the position and velocity of the agents based on personal and global best search patterns of the particle and swarm respectively. Thus, the ambiguity of selecting an acceptable starting point, a trait in GM structures, is not a design issue.

The design variables represent the dimensional positioning of the particles and stored in position vector x_i^D . The PSO operators update the velocity v_i^D at iteration t , as:

$$v_i^D(t) = K[v_i^D(t-1) + c_1 r_1 (pbest_i^D - x_i^D(t-1)) + c_2 r_2 (pbestg - x_i^D(t-1))] \quad \dots (3)$$

Where:

x_i^D position vector;

v_i^D velocity vector: randomly generated at search initialisation;

$pbest_i^D$ best solution achieved by the particle and represented by vector: $pbest_i^D = (pbest_i^1, pbest_i^2, \dots, pbest_i^D)$;

$pbestg$ global best solution collectively achieved by the swarm;

c_1 & c_2 stochastic acceleration terms that pull each particle toward $pbest_i^D$ and $pbestg$ positions respectively;

r_1 & r_2 random numbers in the uniform range [0,1]; and

K constriction factor introduced by Shi and Eberhart⁽²⁴⁾ and applied as an inertia weight term to balance global and local search capabilities of the particles. A large weight factor promotes global search patterns and a small value facilitates a local search process. Shi and Eberhart⁽²⁴⁾ propose K as:

$$K = \frac{2}{|2 - \phi - \sqrt{\phi^2 - 4\phi}|}, \phi = c_1 + c_2, \phi > 4 \quad \dots (4)$$

Through empirical studies, Shi and Eberhart performed test experiments over benchmark test functions and proposed c_1 and $c_2 = 2.05$ thus, $\phi = 4.10$ and $K = 0.729^{25}$.

The update of position vector at iteration t is:

$$x_i^D(t) = x_i^D(t-1) + v_i^D(t) \quad \dots (5)$$

Equations (3-5) have the effect of accelerating the particles towards the weighted sum of the personal and global best with an element of randomness. The iterative search process continues until the user-defined termination criteria is achieved.

The difference between GA and the PSO methodology is that the swarm process does not implement mutation and crossovers, which require additional function evaluations thus, increasing computational time to convergence. Performance comparison between GA and PSO has shown that PSO is sensitive to premature convergence due to the presence of local sub-optima solutions for complex multimodal problems. Stagnant optimisation simulations are due to inefficient solution diversity in the search population. The issue is addressed by increasing the population size of the swarm, but does not guarantee global optima. This option is not preferred as additional function calls are required. Thus, the original PSO search algorithm must be modified to address this demerit.

Table 1
Benchmark validation test functions

Function	Dimensional Search Space	Particle Initialisation Range	Theoretical Global Minima
Ackley	$-32.768 \leq x_i \leq 32.768, i = 1, 2, \dots, n$	$-32.768 \leq x_i \leq 16$	$X^* = (1, \dots, 1), f(x^*) = 0$
Michalewics	$0 \leq x_i \leq \pi, i = 1, 2, \dots, n$	$0 \leq x_i \leq \pi$	$X^* = (2.201, \dots, 1.5710), f(x^*) = -9.66$
Rosenbrock	$-2.048 \leq x_i \leq 2.048, i = 1, 2, \dots, n$	$-2.048 \leq x_i \leq 2.048$	$X^* = (1, \dots, 1), f(x^*) = 0$
Schwefel	$-500 \leq x_i \leq 500, i = 1, 2, \dots, n$	$-500 \leq x_i \leq 500$	$X^* = (1, \dots, 1), f(x^*) = 0$

3.1 Adaptive-mutation particle swarm optimiser

Variants of the original PSO model have been developed and assessed through empirical simulations⁽²⁶⁻⁴²⁾. Search diversity as a function of time has been recognised as a design requirement. Position and velocity vectors are updated with user-defined strategies. A new methodology is proposed which exploits the search experiences of the individual agents in an adaptive sequence.

A probability of mutation method is introduced, which is proportional to the relative positioning of the particles in the swarm. At solution initialisation, the lack of search diversity is not an issue, due to a high sampling space of the particles, thus the probability of mutation is low. As the search progresses and the particles converge to a common region, mutation is adapted proportionally to account for the reduced search diversity. Theoretically, if the swarm is converging to a local region, then mutation will offset this demerit. Alternately, if the swarm is converging to a global region, then mutation will have no influence on the search progress and the positioning of the particles will remain unchanged. Thus, mutation is initiated based on the relative positioning, hence the search experiences of the particles. The original variant of the PSO model is modified and an adaptive time-variant, mutation based PSO algorithm is proposed (AM-PSO). Numeric simulations are performed to validate this concept and to further finalise the following condition.

3.1.1 Numerical experimental results

To validate the effectiveness of the developed search model, numerical experiments are simulated over disparate test problems. Functions applied for validation incorporate both uni and multi-modal solution topology. The Ackley, Michalewics, Rosenbrock and Schwefel functions (Table 1) are included in the numerical validation studies.

For each function, 30 trials are applied and comparisons between the proposed AM-PSO model and the variants developed in the literature^(27,29) are made. The standard deviations of the global fitness and iteration to convergence, represent the robustness of the algorithm and is assessed to measure the performance of the developed method.

The result of the simulation trials over the four test functions is presented in Table 2. A comparative analysis between the performances of the AM-PSO (Table 2) and the reported solutions in the literature^(27,29), indicate the superior search mechanisms of the developed algorithm. The success rate from the 30 runs is 100% for the multimodal Ackley, Michalewics and the Schwefel model (Table 2). The standard deviation of the best solution from the 30 simulations is close to zero, thus signifying the consistency at which AM-PSO converges to the global point. A low iteration standard deviation (Table 2) further shows the consistency at which AM-PSO accelerates to the optimal solution. The test simulations have confirmed that the AM-PSO is well suited for multimodal problems and exhibits acceptable convergence characteristics than the algorithms reported in literature.

Table 2
Test function simulation results

Function	Ackley	Michalewics	Rosenbrock	Schwefel
Worst fitness	4.44e-015	-9.66	3.98	1.97e-004
Fitness	4.44e-015	-9.66	4.30e-002	1.27e-004
Success rate (%)	100	100	97	100
Average fitness				
● Best in literature	3.75e-015 ²⁹	-9.66e+000 ²⁷	6.98e-001 ²⁹	0 ²⁹
● AM-PSO	4.44e-015	-9.66e+000	2.15e-001	2.14e-005
Fitness standard deviation				
● Best in literature	2.13e-014 ²⁹	1.58e-003 ²⁷	1.46e+000 ²⁹	0 ²⁹
● AM-PSO	0	4.88e-005	7.13e-001	2.41e-005
Maximum iteration				
● Literature	30,000 ²⁹	20,000 ²⁷	30,000 ²⁹	30,000 ²⁹
● AM-PSO(standard + mutation)	18,459	6,257	28,623	6,164
Standard PSO operation	9,809	3,792	20,000	3,184
Mutation	8,650	2,465	8,623	2,980
Minimum iteration	1,840	814	1,171	538
Standard PSO operation	975	472	659	306
Mutation	865	342	512	232
Average iteration	2,067	1,844	5,763	1,487
Iteration standard deviation	2,280	911	3,856	769

Table 3
Aerofoil category types for solution space mapping

Aerofoil Type	$[Mach_{min}, Mach_{max}]$	$[Rn_{min}, Rn_{max}] \times 10^6$	$[t/c_{min}, t/c_{max}]$	$[cl_{design,min}, cl_{design,max}]$
a) HALE: HRN	0.10 – 0.50	9.0 – 10.0	0.14 – 0.15	0.10 – 0.46
b) HALE: MRN	0.10 – 0.60	3.80 – 4.0	0.15 – 0.17	0.40 – 0.56
c) NACA	0.70 – 0.75	9.0 – 10.0	0.12 – 0.15	0.30 – 0.70
d) LRN	0.10 – 0.55	0.15 – 0.50	0.073 – 0.15	1.00 – 1.10
e) HRN: High-Speed	0.70 – 0.73	7.0 – 11.0	0.12 – 0.13	0.25 – 0.79

4.0 DESIGN VARIABLES PRE-SCREENING

The aerofoil shape variables for HALE design are analysed. The proposed test methodology is set-up as follows: a) Establish the search space of each variable with an inverse shape optimisation analysis; and b) Establish the importance of each geometry variable to aerofoil aerodynamics hence, the objective function by a quantitative measure.

4.1 Solution search space

The search domain of each variable for HALE aerofoil design is defined to ensure an efficient optimisation simulation. An inverse optimisation process is simulated with the developed AM-PSO algorithm. The inverse process applies a geometrical fitting technique to compute the shape variables of the PARSEC and PARSEC-Modified functions. The objective function J , is defined to minimise the absolute error and is calculated from the permutation of shape variables that $J_{minimise}$, the geometrical difference between target $(y/c)_{target}$ and approximate $(y/c)_{approx}$ shape at each aerofoil chord station M_i , in Equation 6.

PARSEC Variant One: Establish: $r_{le}, y_{te}, t_{eg}, t_{ew}, x_w, y_w, y_{xxw}, x_b, y_b, y_{xx}$
 PARSEC Variant Two: Establish: $r_{leup}, r_{lelow}, y_{te}, t_{egup}, t_{eglow}, t_{ewup}, t_{ewlow}, x_w, y_w, y_{xxu}, x_b, y_b, y_{xx}$

$$J_{min} = \sum_{i=1}^M |(y/c)_{i_{approx}} - (y/c)_{i_{target}}| \dots (6)$$

To graphically illustrate the relationship and data scatter between geometry variables and the intent design goals of the target aerofoil, disparate profile sections are used in the inverse shape optimisation analysis. Aerofoil types examined are classified into five categories: a) HALE: High Reynolds Number (HRN); b) HALE: Medium Reynolds Number (MRN); c) NACA 5-6 series type including symmetrical and non-symmetrical profiles; d) Low Reynolds Number (LRN) sections used in Micro UAVs; and e) HRN at high transonic speeds. The aerodynamic operating performance range and the t/c of the base aerofoils for each category are summarised in Table 3. Shape geometry is correlated with operating conditions ϕ_{op} , which is the summation of aerofoil

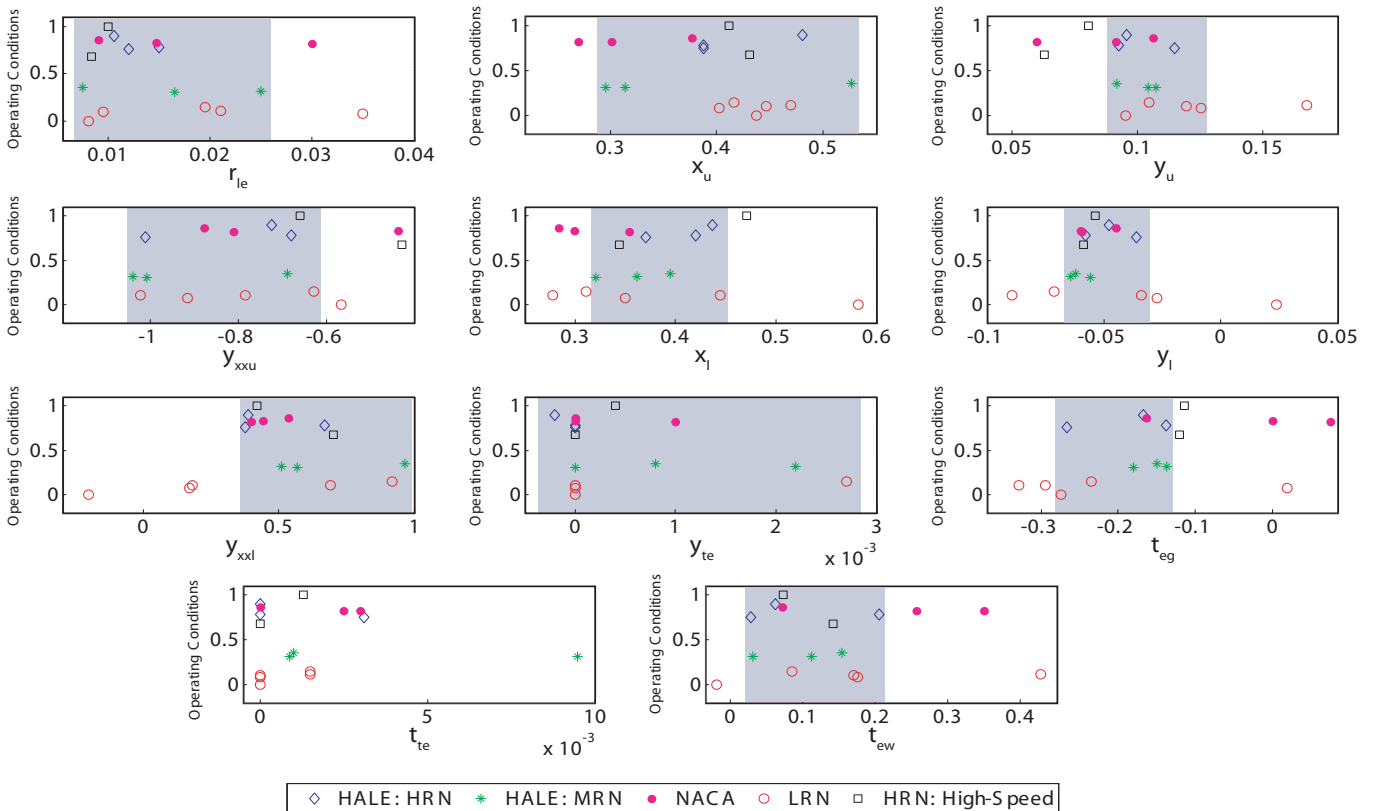


Figure 1. Mapping of solution search space.

characteristics from Table 3 as:

$$\varphi_{op} = |\text{Mach} + R_n + t/c + c_{l_{design}}| \quad \dots (7)$$

The term φ_{op} is originally calculated for each aerofoil, as a function of four operating conditions at the base value. Due to the large deviation in the magnitudes of the four operating units (Equation 7), with R_n measured in 10^6 and M_∞ , t/c and $c_{l_{design}}$ of order one, the results are normalised to range (0,1) for ease-of-inspection. From φ_{op} aerofoil characteristics are related to the shape parameterisation variable. High-speed aerofoils are characterised with sharp nose regions, thus a low r_{le} is expected to avoid premature flow transition about the leading edge due to peak negative pressure coefficients followed by rapid adverse pressure gradients. Thus, aerofoils operating under disparate operating conditions are introduced, with the intention of identifying data dispersion in the mapping analysis as function of φ_{op} . Platforms for HALE missions operate at disparate Reynolds numbers. Thus, the search bounds are established by mapping regions corresponding to HALE-MRN to HRN environments, shaded in Fig. 1.

The bounds are further defined with tolerance to avoid the generation of fish-tailed profiles. It is observed that high-speed sections are characterised with low r_{le} as expected. Low speed sections operating at LRN for Micro-UAV applications require large r_{le} , thus the solution space is not mapped in this region (Fig. 1). A cluster of aerofoils at 0.40-0.50 for x_u is observed for LRN aerofoils. The coefficient is mapped to incorporate the variances of HALE-MRN sections, which are at the extreme ends of the variable range (Fig. 1). The search domain for y_u , y_{xxu} , x_l , y_l , y_{xld} , t_{eg} , t_{ew} (Table 4) is established to integrate HALE aerofoils with MRN to HRN performances, with tolerance to address undulating sections.

For y_{le} , a cluster of profiles with zero variances are observed with extremum profiles limited to a search envelope of (-0.0002, 0.0027). It has been shown that y_{le} has a strong influence on aerofoil (c_l/c_d) at HALE conditions⁽⁴³⁾. Thus, the search envelope is arbitrarily set at (-0.02, 0.02) to exploit the aerodynamic merits of y_{le} to maximise aerofoil efficiency (Table 4). Similarly, a cluster of aerofoils are characterised with zero thickness at the trailing edge with extremum points at 0.0030, for HALE profiles at MRN to HRN operating conditions, thus t_{le} is set accordingly. The search domain of the PARSEC method is summarised in Table 4.

Table 4
PARSEC mapping solution space

Shape Parameter	Minimum	Maximum
r_{le} leading edge radius	0.0065	0.0230
x_u crest of upper surface's x abscissa	0.2873	0.5343
y_u crest of upper surface's y ordinate	0.088	0.125
y_{xxu} curvature at the crest of upper surface	-1.05	-0.620
x_l crest of lower surface's x abscissa	0.310	0.450
y_l crest of lower surface's y ordinate	-0.073	-0.0307
y_{xld} curvature at the crest of lower surface	0.370	0.980
y_{le} trailing-edge ordinate	-0.020	0.020
t_{eg} trailing-edge direction (degrees)	-16.04°	-6.88°
t_{le} thickness at trailing-edge	0	0.0030
t_{ew} trailing-edge wedge angle (degrees)	1.15°	14.73°

4.2 Design variables measure of importance

With the search limits of the design coefficients established, the importance of each variable to HALE aerofoil design is established. The screening technique developed by Morris⁽⁴⁴⁾ is applied, with the

assumption that the objective function is deterministic. The algorithm calculates the effect of each variable and establishes the correlation type between input-output as: a) Negligible; b) Linear and additive; or c) Non-linear or involved in interactions with other factors⁽⁴⁵⁾.

The algorithm measures the sensitivity of the i^{th} variable to aerofoil aerodynamic coefficient as output. Each geometry variable is perturbed one-factor-at-a-time for a discrete number levels p , along each dimension within the defined interval range. Consider a k -dimensional input vector x_i , over a p -level factorial grid, normalised into a unit cube of $(0, 1)^k$. The components of x_i , are a set of values such that $x_i \in \{0, 1/(p-1), 2/(p-1), \dots, 1\}$, for $i = 1, \dots, k$. The output of the objective function y , is established for the baseline value $x \in D$ and the elementary effect $d_i(x)$ of the i^{th} input factor calculated in Equation (8):

$$d_i(x) = \frac{y(x_1, x_2, \dots, x_{i-1} + \Delta, x_{i+1}, \dots, x_k) - y(x)}{\Delta} \quad \dots (8)$$

Where:

y function output/aerodynamic coefficient from flow solver

k number of design variables

Δ $\xi/(p-1)$; $\xi \in \text{IN}^*$, elementary effect step length factor; p = number of discrete levels along dimension $x \in D$ such that $x_i \leq 1 - \Delta$

The distribution of $d_i(x)$ for each x_i is measured at different parts of the design space, to indicate the relative importance of the shape variable of the parameterisation model to aerofoil aerodynamics. The mean μ_m and standard deviation σ_m , of $d_i(x)$ are used as distribution parameters. A large μ_m indicates the shape variable has an important influence on an equating output aerodynamic coefficient. Large σ_m suggests simultaneous interactions between two variables have a strong influence on aerofoil aerodynamics.

4.2.1 Quantitative measure of sensitivity

Morris proposed ranking the importance of variables by the μ_m of $d_i(x)$. Campolongo *et al*⁽⁴⁶⁾ introduced a ranking measure μ^* , which is calculated from the mean of the distribution of the absolute values of the elementary effects, such that $\mu^* = |d_i(x)|$. The proposed methodology addresses the misrepresentation of the magnitude of sensitivity, as a result of opposite signs of the elementary effects for a non-monotonic model.

The effect of PARSEC original and PARSEC-Modified shape variables on aerofoil c_d and $c_{l_{max}}$, is examined. Morris's screening measures of μ_M and Campolongo's μ^* from Equation 8, are applied in Table 5 to rank the importance of aerofoil variables on c_d and $c_{l_{max}}$.

Since x_u influences the chordwise location of the boundary layer transition point, results of the ranking process indicate, x_u has a major influence on c_{db} with the trailing edge wedge having minimal influence (Table 5). The variance of PARSEC coefficients on $c_{l_{max}}$ indicates the importance of the leading edge radius to mitigate early separation leading to premature stall. The variable applied to control the curvature of the crest on the lower surface has minimal activity on $c_{l_{max}}$ (Table 5). The proportion of variance of μ^* (Table 5) of each variable on c_d and $c_{l_{max}}$ is shown in Fig. 2.

The data presented in Table 5 and Fig. 2 is applied to eliminate variables. For HALE aerofoil design, the maximisation of aerodynamic efficiency is a requirement, thus drag minimisation a primary goal. This is also coupled with the goal of attaining acceptable maximum lift performances with transition located about the leading edge. Thus, $c_{l_{max}}$ is not dependent on the achievement of laminar flow and is also related to take-offs from short runways and safety considerations to stall at landing speeds. The pre-screening analysis indicated that t_{ew} is least important to c_{db} , while the differences between the 10th and 11th ranked

Table 5
PARSEC variables measure of importance on c_d and c_{lmax}

c_d					c_{lmax}				
PARSEC	μ_M	μ^*	σ_M	Ranked μ^*	PARSEC	μ_M	μ^*	σ_M	Ranked μ^*
x_u	0.0005	0.01	0.0231	1	r_{le}	0.1208	0.4749	1.1325	1
y_u	0.0004	0.0042	0.0119	2	y_l	-0.0862	0.3584	1.2426	2
t_{eg}	-0.0015	0.0042	0.0325	3	x_u	0.0774	0.3464	1.2963	3
r_{le}	-0.0001	0.003	0.0109	4	y_{xxu}	-0.1869	0.3015	2.1501	4
y_{te}	-0.001	0.0028	0.0109	5	y_u	0.0863	0.2856	1.8901	5
y_l	0.0017	0.0027	0.0312	6	y_{te}	-0.0591	0.2371	1.2486	6
y_{xxu}	0.0002	0.0021	0.0061	7	t_{te}	-0.0095	0.2344	1.0978	7
y_{xxl}	-0.0001	0.0017	0.0084	8	x_l	-0.0147	0.2317	0.8413	8
x_l	0.0008	0.0014	0.0072	9	t_{eg}	-0.017	0.1899	0.4878	9
t_{te}	-0.0001	0.0009	0.0069	10	t_{ew}	0.0245	0.1709	0.6499	10
t_{ew}	0.0003	0.0009	0.0059	11	y_{xxl}	0.0292	0.158	0.5396	11

variable for c_{lmax} relating t_{ew} and y_{xxl} respectively is minimal (Table 5). As drag minimisation is assumed to be a primary design objective and with t_{ew} indicating minimal influence on c_d and c_{lmax} the parameter is eliminated from shape optimisation simulations. The trailing edge thickness is also eliminated due to its minimal contribution to drag (Table 5 and Fig. 2). More importantly, the variable is omitted to simplify the geometry meshing process and the optimisation computation performance. A finite thickness will require greater number of cell elements to resolve aerofoil wake, which will significantly increase the computation time to convergence. Thus, a low contribution to c_d and to avoid a large grid cell count, t_{te} is eliminated from the optimisation simulation.

Similarly the quantitative measure of sensitivity is also applied to the PARSEC-Modified method. The trailing edge angle on the lower surface teg_{low} , is identified as least important. A contribution of 4% to c_d and 9% variance to c_{lmax} is computed. Thus, teg_{low} is eliminated from the design space by the PARSEC-Modified method.

5.0 AEROFOIL OPTIMISATION

The target validation aerofoil is NASA’s NLF(1)-0416 planform designed for light, single-engine, general aviation airplanes. The planform was designed with the following objectives:

1. The c_{lmax} at $R_n = 3.0 \times 10^6$ must be greater than 1.76. The maximum lift coefficient should not decrease with transition fixed at the leading edge due to surface contamination by insect remains; and
2. Obtain low profile drag-coefficients at $R_n = 4.0 \times 10^6$ for cruise target lift coefficient of 0.40 and climb lift coefficients of $c_l^T = 0.50 - 1.00$.

The following constraints were applied in the design:

1. Extent of the favorable pressure gradient $d_{cp}/d_x < 0$, on aerofoil upper surface at cruise c_l must not exceed 30-percent chord;
2. Aerofoil t/c must be greater than 12%; and
3. Pitching-moment coefficient at zero lift c_{m0} , must be $c_{m0} \geq -0.10$

A favorable pressure gradient on the upper surface is required up to the maximum extent allowed by the constraint of $(x/c)_{up} \leq 0.30$. Aft of 0.30c, a short region of slightly adverse pressure gradient is required to promote efficient transition from laminar to turbulent flow. This ensures that the initial slope of the pressure recovery is relatively shallow. This short region is then followed by a steeper, concave pressure recovery, which produces lower drag and has less tendency to separate than the corresponding linear or convex pressure recovery.

The extent of aerofoil camber is limited by the pitching-moment constraint ($c_{m0} \geq -0.10$), which is defined to maximise c_{lmax} .

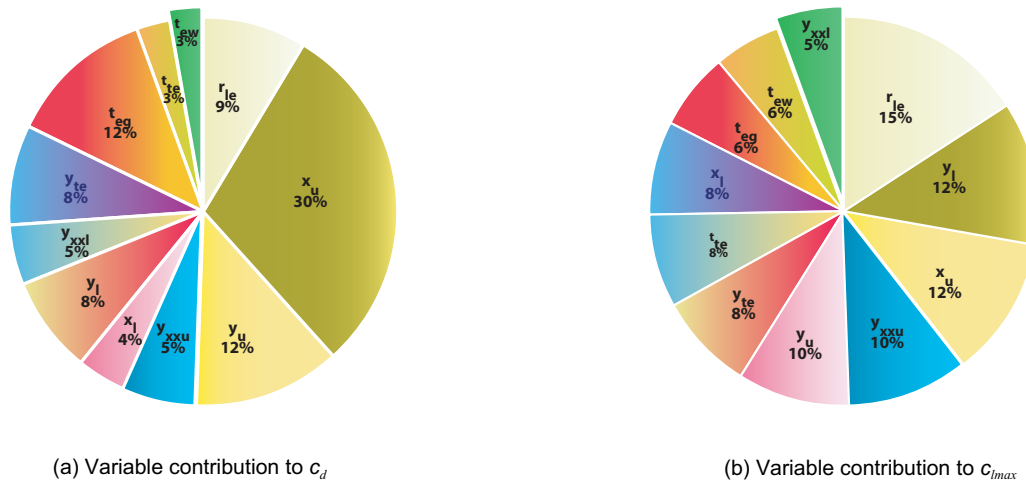
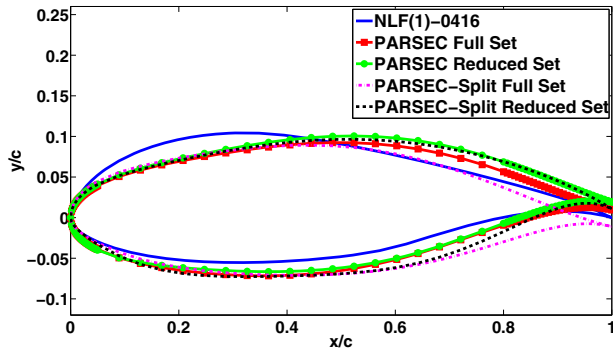


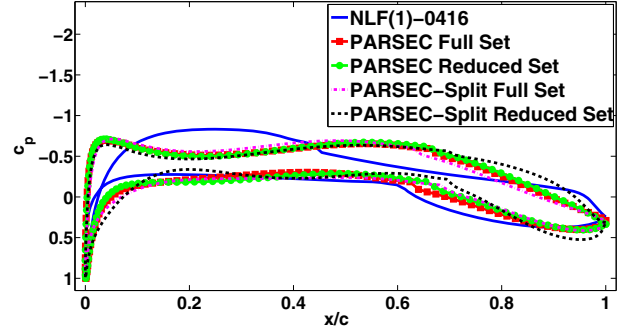
Figure 2. Proportional to total variance.

Single-Point Optimisation by PARSEC & PARSEC-Modified Functions



(a) NLF(1)-0416 aerofoil and single-point optimised

Single-Point Optimisation Coefficient of Pressure Distribution by PARSEC & PARSEC-Modified Functions

(b) C_p distribution of NLF(1)-0416 aerofoil and single-point optimisation results at cruise c_l 0.40

Single-Point Optimisation Drag Polar by PARSEC & PARSEC-Modified Functions

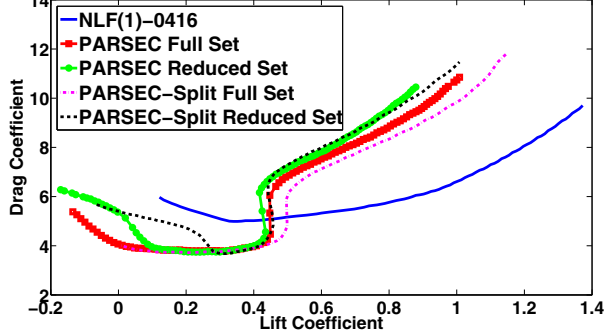
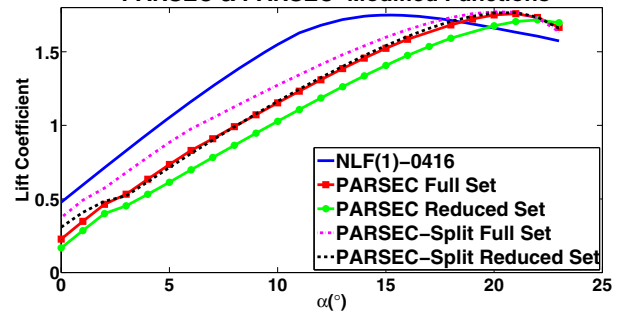
(c) Drag polar of NLF(1)-0416 and single-point optimisation results at $R_n = 4.0 \times 10^6$ Single-Point Optimisation of c_{lmax} by PARSEC & PARSEC-Modified Functions(d) c_{lmax} of NLF(1)-0416 and single-point optimisation results at $R_n = 3.0 \times 10^6$

Figure 3. Single-point optimisation.

5.1 Parallel computing set-up

Automated computing optimisation architecture, with the integration of the DNO components is developed. Heuristic search models are adaptable to parallelism and an efficient computation model is developed to accelerate AM-PSO simulation with MATLAB's distributed computing toolbox. Shell scripts are prepared in MATLAB to distribute each particle to a processing unit on a super-computing facility.

5.2 Optimisation set-up

The solution to aerofoil design problem is represented by a vector of shape variables x , for the PARSEC and PARSEC-Modified functions. The angle-of-attack α , is not treated as a design variable, since XFOIL has a built-in trimming function that calculates the angle required for target lift.

The shape optimisation problem for validation is defined as a single objective, with drag minimisation a primary requirement, with constraint on c_{lmax} . The design objectives and constraints for the NLF(1)-0416 design (Section 5), are transformed into the search algorithm as follows:

$$\text{At } R_n = 4.0 \times 10^6$$

minimise c_d

Subject to:

$$\Rightarrow d_{cp}/d_x(x, \alpha, M_\infty) \leq 0.30c$$

$$\Rightarrow c_{m0}(x, \alpha, M_\infty) \geq -0.10$$

$$\Rightarrow t/c_{max}(x) \geq 0.12$$

$$\text{At } R_n = 3.0 \times 10^6$$

$$\Rightarrow \text{Subject to: } c_{lmax}(x, \alpha_{max}, M_\infty) \geq 1.76$$

Constraints are applied by penalty functions to the objective function to ensure minimum drag performance is not compensated by a constraint violated design. A static penalty function is introduced and is normalised to (0,1) if the aerodynamic and/or geometric constraints (Section 5) are violated such that:

$$f_p(x) = (x) + \sum_{j=1}^{\eta_{con}} c_j \quad \dots (9)$$

Where:

f_p fitness as a result of penalty

c_j expected maximum cost to repair constant j (i.e alter x so it is feasible); normalised to (0,1)

η_{con} number of constraints

At each search evolution the aerodynamic and geometric quantities of the candidate solution are calculated. The summation of c_j for each constraint is added to the overall fitness to penalise the particle for respective constraint violation.

5.3 HALE optimisation with AM-PSO

HALE aerofoil optimisation with single and multi-point designs are simulated. Single-point performances minimise drag at cruise $c_l^T = 0.40$.

As fitness for constraint violation is normalised to range (0,1), the magnitude of c_d is manipulated to reflect an even contribution of the objective term, relative to the penalty magnitude. Thus, a multiple of 100 to c_d is applied to ensure the contribution of drag is not diminished by the normalised magnitude of the penalty magnitude. The objective is substituted into the search algorithm in Equation (10):

$$\text{minimise: } 100 \times c_d \quad \dots (10)$$

For multi-point designs, drag minimisation at the operating spectrum of the lift coefficient envelope for climb and cruise coefficients is used. The flight points selected are cruise $c_l^c = 0.40$ and climb $c_l^c = 1.00$. The objective function in relation to the search algorithm is defined as follows:

$$\text{minimise: } 100 \times c_{d_{cruise}} + 100 \times c_{d_{climb}} \quad \dots (11)$$

5.3.1 Single-point optimisation

The single-point optimisation (Equation (10)) is simulated with AM-PSO. Aerofoil geometry (Fig. 3(a)) and aerodynamic performance comparisons (Fig. 3(b)-3(d)) between validation NLF(1)-0416 profile and shape optimisation simulations is presented in Fig. 3.

A direct comparison between validation and AM-PSO aerofoil shapes shows that simulation results are characterised with extended x_u and y_l coefficients (Fig. 3(a)). The trailing edge ordinate is also unique for each shape (Fig. 3(a)). The results are representative of the theoretical principles of HALE aerofoil design, with the maximum thickness point in excess of 0.50c (Fig. 3(a)). Thus, extended regions of adverse pressure gradients are observed (Fig. 3(b)). Transition is delayed and is in excess of 0.60c on both upper and lower surfaces compared to 0.43c and 0.57c on suction and pressure surfaces respectively for the NLF(1)-0416 (Fig. 3(b)). Delayed transition with extended x_u , minimises skin-friction drag. The drag performances are compared in Fig. 3(c). A 'drag bucket' at objective c_l^c of 0.40 is observed (Fig. 3(c)). Drag at the specified flight condition is the 'global' solution to the single-point problem and is minimal compared to the validation case. Elsewhere drag is significantly higher with rapid performance degradation at off-design conditions (Fig. 3(c)). The performance is related to the demerits of the single-point based design approach. The aerodynamic and geometrical properties of the base and optimised aerofoils is summarised in Table 6.

The results indicate that the geometrical constraint of $t/c > 0.12$ is satisfied by all designs. The maximum camber of the simulation shapes is lower than the validation profile and a higher AOA is required to compensate for the low camber to achieve target cruise c_l (Table 6). A reduction of drag in excess of 20% is observed across the simulation data (Table 6). With an increase of polynomial order for aerofoil shape representation, drag decreases proportionally. A full set of PARSEC variables has lower drag ($c_d = 0.00398$) compared to the analysis with t_{ew} eliminated ($c_d = 0.00399$). A percentage difference of $\approx 0.25\%$ is

minimal. Thus, the effect of eliminating t_{ew} from the pre-screening analysis due to a low drag contribution is validated. Overall, the original PARSEC method indicates a drag reduction in excess of $\approx 20\%$ compared to the base validation aerofoil.

The modified variant of the PARSEC method, with thirteen variables exhibits the lowest drag ($c_d = 0.00390$), equating to a reduction of $\approx 22\%$ in comparison to the base aerofoil. Drag increases slightly ($c_d = 0.00392$) with the elimination of teg_{low} (Table 6) with a percentage difference of $\approx 0.50\%$ between the full and reduced sets. The minimal difference validates the proposed design variable pre-screening test methodology (Section 4.2.1).

The effect of varying the polynomial order of the aerofoil shape function, on $c_{l_{max}}$ is observed (Table 6). An increase in design variable population size has the merit of increasing the $c_{l_{max}}$ of the optimised aerofoils (Table 6). The original PARSEC model with a full set of design variables matches the $c_{l_{max}}$ of the base aerofoil with a minimal increase of $\approx 0.50\%$ (Table 6). By the sensitivity analysis, it was shown that t_{ew} has a variance of 6% to $c_{l_{max}}$ compared to the least important factor, y_{xst} which exhibits a 5% contribution (Fig. 2(b)). The coefficient t_{ew} was eliminated based on the minimal contribution to drag only (Fig. 2(a)). The equating influence of t_{ew} on $c_{l_{max}}$ was not considered. As a result, the $c_{l_{max}}$ of the PARSEC reduced-set decreases to 1.72 in comparison to 1.76 with full ten design variables. This equates to a percentage difference of $\approx 2\%$ between the two sets. The $c_{l_{max}}$ of the reduced method violates the constraint $c_{l_{max}} > 1.76$ (Section 5.2). Thus, a design compromise of reduced drag and $c_{l_{max}}$, by eliminating t_{ew} is established.

The PARSEC-Modified function with a full set of design variables exhibits the highest $c_{l_{max}}$ and equates to an increase of $\approx 1\%$ in comparison to the validation profile (Table 6). For the reduced set, $c_{l_{max}}$ is marginally lower than the full set, yet greater than the base aerofoil. Since teg_{low} simultaneously exhibits the lowest variance to c_d and $c_{l_{max}}$, the percentage differences of the aerodynamic performances, between the full and reduced sets is minimal.

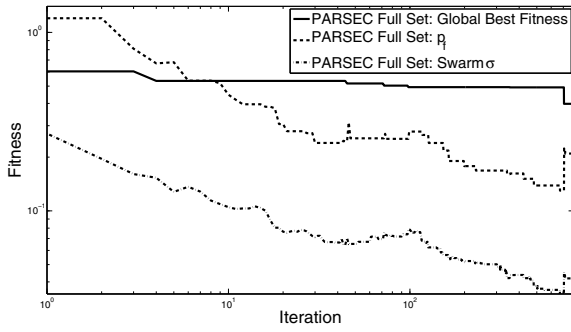
Solution termination is measured by the search performance of $pbestg$ including the personal best fitness range p_f . The quantity p_f is computed by the absolute fitness difference of the worst and best performing particles in the swarm. To further incorporate the search patterns of the population, a third measure based on the fitness spread of the swarm is presented, by σ_r . The proposed termination measures are defined to balance between a premature and conservative search process.

In Fig. 4, an extended region of a stagnant global best solution as a function of iteration time is observed. Concurrently, p_f and σ_r deviate simultaneously thus, illustrating an active search history within the swarm. For the PARSEC original method with a full set of design variables (Fig. 4(a)), the three termination quantities $pbestg$, p_f and σ_r indicate a stagnant search process from the 705th iteration. Repeat of the simulation with t_{ew} eliminated indicates stagnation from the 522nd generation (Fig. 4(b)). Thus, convergence is achieved with $\approx 26\%$ fewer iterations between the full and reduced sets (Figs 4(a)-4(b)).

Table 6
Single-point optimisation results

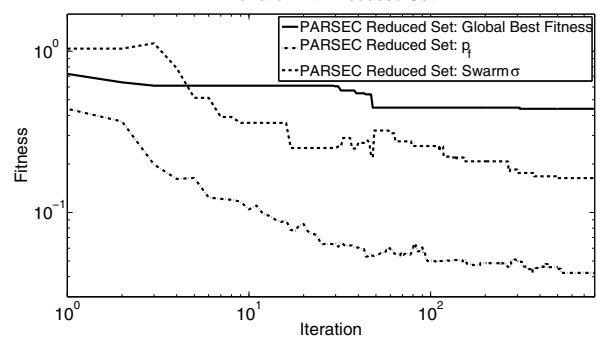
Aerofoil	t/c	Max Camber	c_l	AOA	c_d	% c_d Gain	$c_{l_{max}}$ $R_n = 3 \times 10^6$	% $c_{l_{max}}$ Gain	d_{cp}/d_x	C_{m0}
NLF(1)-0416	0.16	0.025	0.40	-0.695	0.00502	-	1.7500	-	0.2493	-0.0994
PARSEC (Full Set)	0.16	0.016	0.40	1.432	0.00398	-↓20.72	1.7589	+↑0.51	0.0388	-0.0822
PARSEC (Reduced Set - t_{ew})	0.163	0.016	0.40	1.989	0.00399	-↓20.52	1.7165	-↓1.91	0.0408	-0.0839
PARSEC - Split (Full Set)	0.160	0.014	0.40	0.203	0.00390	-↓22.31	1.7717	+↑1.22	0.0542	-0.0639
PARSEC - Split (Reduced Set - teg_{low})	0.165	0.019	0.40	0.910	0.00392	-↓21.91	1.7661	+↑0.91	0.0432	-0.0969

Single-Point Optimisation: Analysis of Solution Convergence by PARSEC Function with Full Set



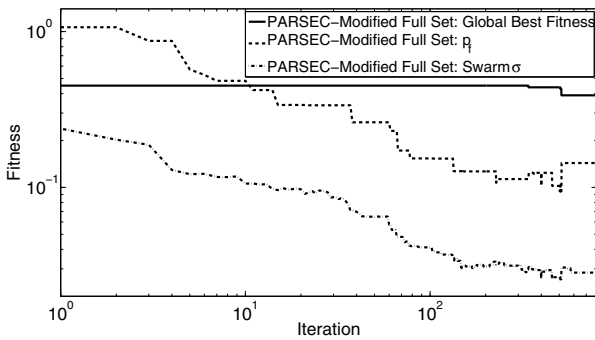
(a) Single-point termination PARSEC full set

Single-Point Optimisation: Analysis of Solution Convergence by PARSEC Function with Reduced Set



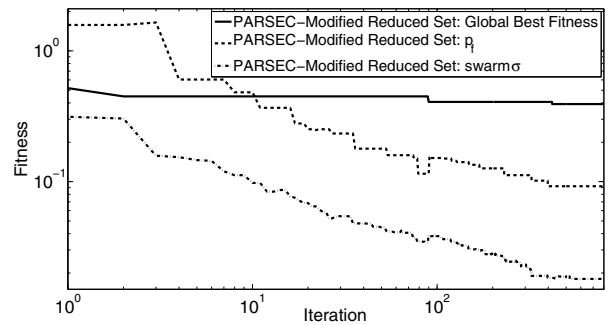
(b) Single-point termination PARSEC reduced set

Single-Point Optimisation: Analysis of Solution Convergence by PARSEC-Modified Function with Full Set



(c) Single-point termination PARSEC-modified full set

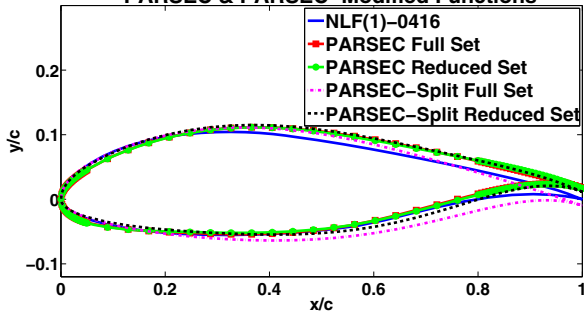
Single-Point Optimisation: Analysis of Solution Convergence by PARSEC-Modified Function with Reduced Set



(d) Single-point termination PARSEC-modified reduced set

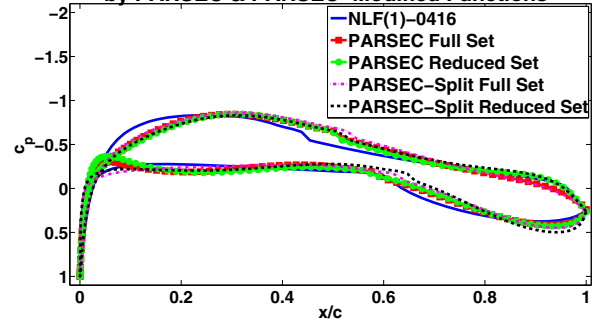
Figure 4. Single-point optimisation: analysis of solution convergence by AM-PSO method with PARSEC & PARSEC-modified variants.

Multi-Point Optimisation by PARSEC & PARSEC-Modified Functions



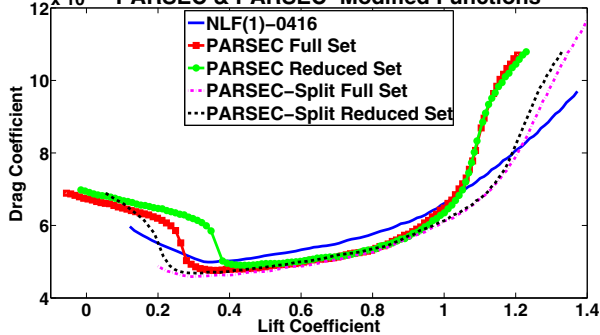
(a) NLF(1)-0416 aerofoil and multi-point optimised shapes.

Multi-Point Optimisation Coefficient of Pressure Distribution by PARSEC & PARSEC-Modified Functions



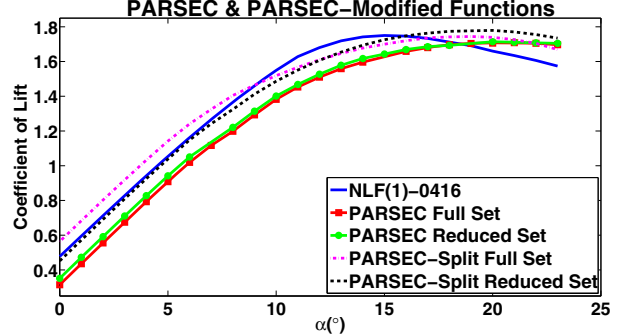
(b) C_p distribution of NLF(1)-0416 Aerofoil and multi-point optimisation results at cruise c_i 0.40.

Multi-Point Optimisation Drag Polar by PARSEC & PARSEC-Modified Functions



(c) Drag polar of NLF(1)-0416 and multi-point optimisation results at $Re_n = 4.0 \times 10^6$.

Multi-Point Optimisation of c_{lmax} by PARSEC & PARSEC-Modified Functions



(d) c_{lmax} of NLF(1)-0416 and multi-point optimisation results at $Re_n = 3.0 \times 10^6$.

Figure 5. Multi-Point Optimisation Results.

Table 7
Multi-point optimisation results

Aerofoil	t/c	Max Camber	c_l	AOA	c_d	% c_d Gain	c_{lmax} $R_n = 3 \times 10^6$	% c_{lmax} Gain	d_{cp}/d_x	C_{m0}
NLF(1)-0416	0.16	0.025	0.40	-0.695	0.00502	-	1.7500	-	0.2493	-0.0994
PARSEC (Full Set)	0.165	0.022	0.40	0.675	0.00479	-↓4.58	1.7084	-↓2.38	0.2909	-0.0951
PARSEC (Reduced Set - t_{ew})	0.163	0.024	0.40	0.355	0.00495	-↓1.40	1.7137	-↓2.07	0.3049	-0.1037
PARSEC - Split (Full Set)	0.175	0.027	0.40	-1.396	0.00464	-↓7.57	1.7440	-↓0.34	0.3056	-0.0901
PARSEC - Split (Reduced Set - teg_{low})	0.170	0.026	0.40	-0.484	0.00473	-↓5.78	1.780	+↑1.69	0.3017	-0.0978

By eliminating teg_{low} in the PARSEC-Modified method, the global best stagnates at the 420th iterate, p_f at 398th and finally σ_f at 523rd generation (Fig. 4(d)). By eliminating teg_{low} , the aerodynamics of the final solution is compromised by $\approx 0.50\%$ (Table 6) in comparison to the full set, for c_d and c_{lmax} . The potential computational time savings are significant thus, validating the effectiveness of eliminating un-important design variables by a pre-screening study.

5.3.2 Multi-point optimisation

To address the demerits of the single-point design approach, a multi-point methodology is applied to minimise drag over an extended lift coefficient flight envelope covering climb and cruise. The problem is formulated by taking the summation of the drag performances at the extremum flight conditions (Equation (11)). Drag minimisation at climb and cruise is specified which equates to a c_l^f of 1.00 and 0.40 respectively. The importance of drag at each c_l^f is weighted equally ($w_i = 1$). Similar to the single-point analysis, the effect of applying the PARSEC and PARSEC-Modified functions with a full and reduced set of design variables is examined and the results presented in Fig. 5.

The aerofoil shapes (Fig. 5(a)) of the multi-point design match closely to the validation case. This suggests that multi-point designs are adapting to the flight conditions of the baseline shape; minimise drag over an extended lift coefficient envelope. In comparison to the baseline shape, multi-point exhibits delayed flow transition (Fig. 5(b)) but not to the extent observed in single-point designs (Fig. 3(b)). The observed performance indicates a design compromise between the two flight conditions.

The overall effect of the multi-point design on drag is presented in (Fig. 5(c)). An extended 'drag bucket' is observed in comparison to single-point design, which was localised about the cruise c_l^f (Fig. 3(c)). In multi-point simulations, favorable drag performance is observed over an extended input c_l^f range covering climb and cruise. The drag performances of all aerofoils achieved by the AM-PSO simulations are lower than the baseline shape (Fig. 5(c)). Thus, the merit of the multi-point approach on aerofoil drag minimisation is validated. At off-conditions for $c_l < 0.40$ and $c_l > 1.00$ (Fig. 5(c)), the performance degrades significantly. The aerodynamic and geometrical properties of the base and optimised aerofoils is summarised in Table 7.

A drag reduction of 1% ~ 7% is observed across the optimal shapes generated at cruise c_l^f in comparison to the validation aerofoil. The overall drag reduction magnitude does not match single-point designs where drag minimisation in excess of $\approx 20\%$ was computed. The results established signify a design compromise between the two flight conditions. The best drag at cruise c_l^f with multi-point design by the PARSEC-Modified variant ($c_d = 0.00464$) is $\approx 16\%$ greater than the minimum drag performance by the single-point design ($c_d = 0.00390$). Thus, a design compromise between multi and single-point designs is evident.

An increase in the polynomial order applied for aerofoil shape generation, increases the magnitude of drag reduction (Table 7). Drag

reduction of $\approx 7.5\%$ is computed with the PARSEC-Modified method utilising the full set of thirteen variables (Table 7). Drag improvement in comparison to baseline shape is reduced to 6% with the elimination of teg_{low} (Table 7).

The c_{lmax} for multi-point designs is $\approx 0.5\%$ lower than the baseline profile. Thus, the performance of c_{lmax} is sensitive to drag minimisation at multiple flight conditions as opposed to single-point designs. The PARSEC original method with full and reduced set of design coefficient, exhibit lower c_{lmax} than the equivalent variant model. Thus, an increase in the order of the polynomial shape function, increases c_{lmax} of the optimal shape accordingly (Table 7).

The constraint relating to the extent of the favorable pressure gradient is observed to converge about the baseline value of the NLF(1)-0416 aerofoil for all cases examined (Table 7). For three out of the four simulations, the minimum chord location of d_{cp}/d_x constraint (Section 5), is violated with minimal deviation from the user-specified design requirement (Table 7). The d_{cp}/d_x has shifted aft of the leading edge in comparison to single-point designs to compensate for delayed flow transition at two disparate flight conditions instead of a uni-based design operation. Thus, multi-point designs are characterised by aft pressure loadings (Fig. 5(b)) relative to single-stage designs (Fig. 3(b)), for chord regions bounded by $x/c \approx 0.70 - 1.00$.

The flight performance at climb c_l^f is presented in Table 8. A maximum reduction of $\approx 7.50\%$ is observed with the full set of design variables by the PARSEC-Modified function (Table 8). Drag at climb is lower with the PARSEC-Modified method in comparison to the original parameterisation model. Thus, an increase in design variable population size has an effect of decreasing drag accordingly.

For the PARSEC-Modified functions, the effect of eliminating teg_{low} from the optimisation analysis has an effect of increasing drag at climb (Table 8) and cruise (Table 7), in comparison to the original set. At climb, a drag rise of $\approx 0.20\%$ is calculated by a simulation with twelve design coefficients ($c_d = 0.00613$) compared to an optimisation with thirteen variables ($c_d = 0.00612$). The percentage difference is assumed to be negligible. At cruise, the percentage increase as a result of variable

Table 8
Multi-point optimisation results – flight condition at $c_l^f = 1.00$

Aerofoil	Max Camber	c_l	AOA	c_d	% c_d Gain
NLF(1)-0416	0.025	1.00	4.479	0.00661	—
PARSEC (Full Set)	0.022	1.00	5.798	0.00648	-↓1.97
PARSEC (Reduced Set - t_{ew})	0.024	1.00	5.496	0.00635	-↓3.93
PARSEC - Split (Full Set)	0.027	1.00	3.677	0.00612	-↓7.41
PARSEC - Split (Reduced Set - teg_{low})	0.026	1.00	4.60	0.00613	-↓7.26

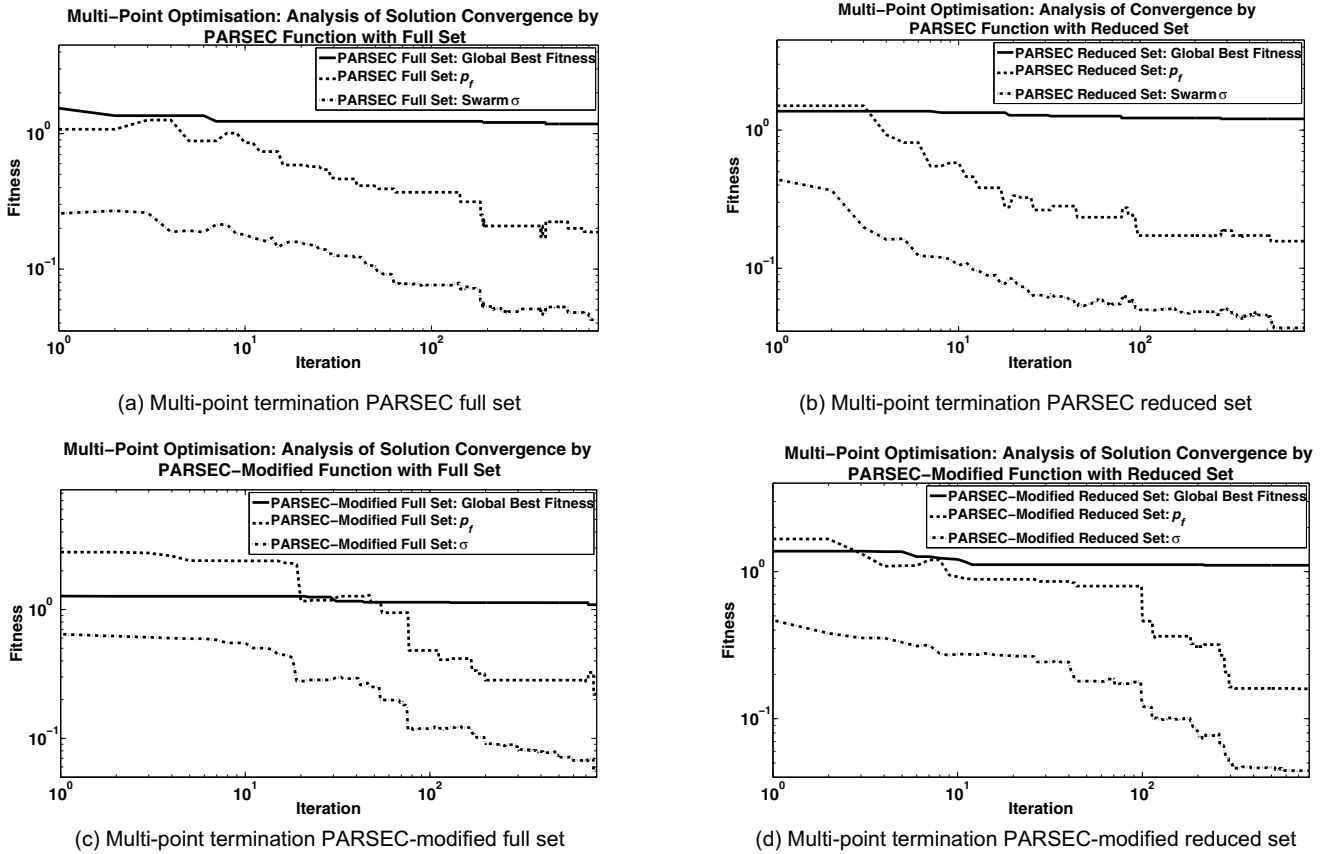


Figure 6. Multi-point optimisation: Analysis of solution convergence by AM-PSO method with PARSEC & PARSEC-modified variants.

elimination is $\approx 2\%$. Even with design variable elimination, the drag performances of the optimal shape generated by the AM-PSO method are favorable in comparison to the baseline NLF(1)-0416 aerofoil. The effect of variable elimination, on search iteration to convergence is examined in Fig. 6.

The PARSEC methodology with a full set of design variables (Fig. 6(a)) converged at the 716th iterate. The global best and p_f converged at the 410th and 659th iterate respectively, followed by the convergence of σ , at the 716th iteration (Fig. 6(a)). A stagnant global best solution extending over 219 iterations from the 190th – 409th evolution is observed (Fig. 6(a)). If solution convergence based on the performance of p_{best} only is defined, then this will result in premature convergence and the generation of a sub-optima solution. Thus, the novel approach of integrating multiple convergence measures, based on the search patterns of the swarm, to avoid premature search termination is validated.

The termination measures for the PARSEC methodology with t_{ov} eliminated, converged at the 544th iterate (Fig. 6(b)). In comparison to a simulation with a full set of design variables, 172 fewer (716-544), iterations are required.

The PARSEC-Modified method with thirteen variables converges at the 774th iterate (Fig. 6(c)). The defined termination parameters remain constant from the 774th evolution up to the maximum iteration count of 800 (Fig. 6(a)) thus, indicating a converged state. In comparison, the simulation with twelve design coefficients converges at the 661st search evolution (Fig. 6(d)). A reduction of 113 design iterations between the two simulations (774 – 661), results in significant computational time savings. Thus, the effectiveness of eliminating un-important design variables on computational time to convergence, is validated.

5.4 Validation of AM-PSO optimisation results

The accuracy of the AM-PSO optimisation results (Section 5.3) is validated with the resolution of the variable values about the optima,

verified. The shape coefficients of the final aerofoil are perturbed one-factor-at-a-time, within an identified test envelope, over user-defined test increments. The flow solver is simulated and the aerodynamic and constraint data stored. A data-mining technique is applied to qualitatively represent solution topology about the optima region by self-organising maps (SOMs), proposed by Kohonen⁽⁴⁷⁾ and implemented in Viscosity SOMine software package⁽⁴⁸⁾. From the maps, a two-dimensional representation of multi-dimensional data is presented. Thus, solution topology with minimum drag conforming to user-defined constraints, about the established optima is qualitatively established. A comparative analysis between c_{dmin} , by the AM-PSO and the perturbation method is performed to assess the validity of the AM-PSO solution.

The aerodynamic and constraint performance in the maps is ordered by the Kohonen algorithm⁽⁴⁷⁾, where data clustering is assigned by prioritising important shape and flow features. In aerofoil shape optimisation, the objective function relating to c_{db} with constraint on c_{lmax} is prioritised. Thus, the equating PARSEC-Modified shape variables are clustered based on the similarity of the attribute values, to the important design features. Hence, the quantities c_d and c_{lmax} influence the clustering c_p , c_{m0} and flow transition on upper and lower surfaces. The equating constraint violation magnitudes are also grouped accordingly. Thus, the maps will qualitatively represent regions with minimum c_d and high c_{lmax} relative to the identified features, through two-dimensional maps.

The feasibility of the AM-PSO solution is further evaluated by a hybrid optimisation process. The solution by the global AM-PSO method is integrated as search initialisation, into a gradient based optimiser. Minimum drag performance by the hybrid approach is assessed and compared to stand-alone AM-PSO simulation. The optima solution to the hybrid approach, is re-validated by the proposed data-mining technique to further verify the feasibility of the solution.

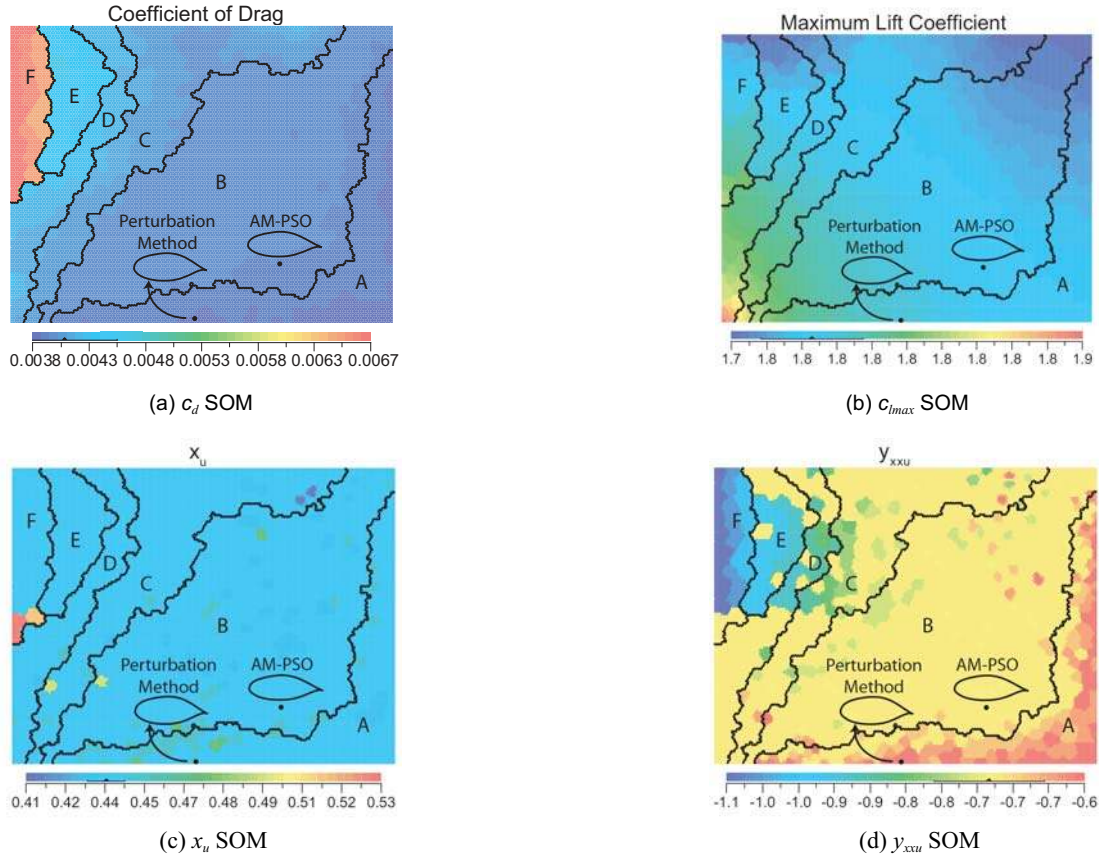


Figure 7. Single-point AM-PSO Solution topology by SOMs.

5.4.1 Single-point design

A. Qualitative representation of AM-PSO results

The PARSEC-Modified variables to the single-point solution in Table 6, are applied in the perturbation methodology. Since low-fidelity solvers are applied, a large population of test aerofoils are examined, with acceptable computation turn-over. A test matrix of 9,261 aerofoils are generated, by independently perturbing each coefficient over 21 intervals within the search limits from Section 4.1. Non-converged simulations are excluded to avoid misinterpretation of the search topology. The clustering of c_d and c_{lmax} , relative to the shape parameters x_u and y_{xcu} are qualitatively represented in Fig. 7.

The maps are clustered by partitioning c_d of the test aerofoils into six groups (A-F). Aerofoils in cluster A are characterised with a low minimum/maximum drag ratio performance (Fig. 7(a)). The magnitude of the lower and upper limits of c_d increases as the data spans from the lower right (cluster A) to the upper left (cluster F) of the map in Fig. 7(a). The equating relationship of c_d in the clusters, to c_{lmax} and shape variables x_u and y_{xcu} , is represented in Figs 7(b-d) respectively. The solution of the AM-PSO method to single-point design (Table 6) is in

cluster B (Fig. 7(a)). From the maps, it is established that the solution in cluster B is not the true optima as aerofoils with lower c_d are present in cluster A. Hence, the variables of the AM-PSO require further validation.

The perturbation method indicates solution region with lower c_d (cluster A), which have not been exploited by the global optimiser. The aerofoil with the lowest c_d by the perturbation method is represented in cluster A. Aerofoil contour variations between the AM-PSO generated solution and the profile in cluster A, is isolated to changes in x_u and y_{xcu} (Fig. 7(c-d)). The profile in cluster A has lower drag due to an extended x_u in comparison to the shape in cluster B, which has the affect of delaying flow transition thus, maintaining extended regions of laminar flow on the upper surface. The variable y_{xcu} , has also not converged to the true optima in the AM-PSO simulations. Low drag aerofoil in cluster A (Fig. 7(a)), corresponds to an increase in y_{xcu} , in comparison to the shape presented in cluster B, where y_{xcu} is lower (Fig. 7(d)). Sensitivity analysis indicates that y_{xcu} is highly ranked on the level-of-importance scale, in the contribution to c_d . Thus, acceptable convergence of the variables is required so that the optimal shape can be validated.

Table 9
Single-point results by AM-PSO, AM-PSO Perturbation and hybrid optimisation approach

Method	t/c	Max camber	c_l	AOA	c_d	% c_d Gain	c_{lmax} $R_n = 3 \times 10^6$	% c_{lmax} Gain	d_{cp}/d_x	C_{m0}
NLF(1)-0416	0.16	0.025	0.40	-0.695	0.00502	—	1.7500	—	0.2493	-0.0994
AM-PSO	0.160	0.014	0.40	0.203	0.00390	-↓22.31	1.7717	+↑1.22	0.0542	-0.0639
AM-PSO Perturbation	0.160	0.015	0.40	0.016	0.00376	-↓25	1.7804	+↑1.71	0.0658	-0.0697
Hybrid AM-PSO / GM	0.160	0.019	0.40	0.495	0.00362	-↓28.88	1.7467	-↓0.20	0.0978	-0.0969

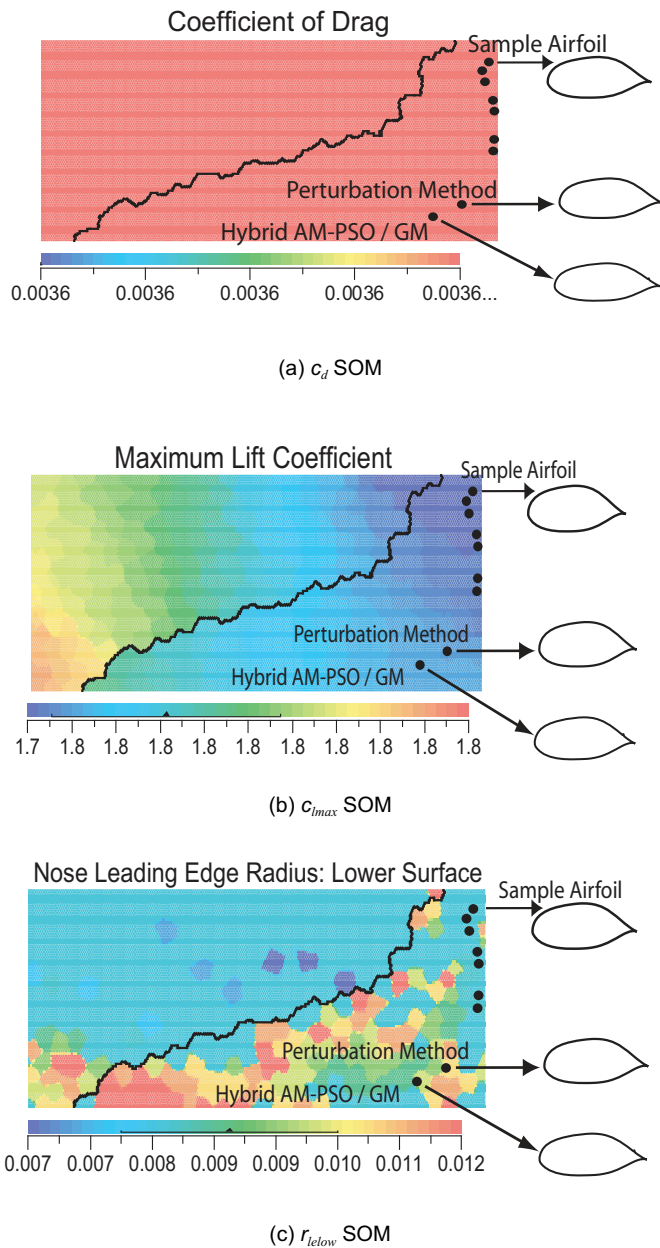


Figure 8. Single-point solution topology validation by SOMs.

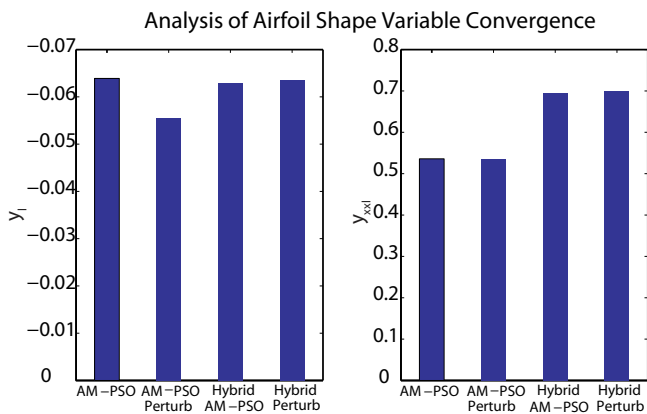


Figure 9. Convergence of y_l and y_{xcl} airfoil shape variables.

B. Results validation by hybrid optimisation

Qualitative representation of AM-PSO results (Section 5.4.1), indicates the solution is within a search topology bounded by low c_d performance (Fig. 7(a)). The global search method does not converge to the true optima with aerofoils in cluster A ignored during the search optimisation process (cluster A in Fig. 7(a)). Gradient based methods are applied to address this issue. A constrained minimisation algorithm using a trust region method is introduced. The AM-PSO single-point result is integrated into the gradient based approach, for search initialisation. Aerofoil performance by the AM-PSO, including the perturbation of the AM-PSO solution (Section 5.4.1) and the hybrid optimisation approach, is presented in Table 9:

The hybrid optimisation approach indicates a $\approx 7\%$ reduction in c_d (0.00362), from the stand-alone AM-PSO method (0.00390) and $\approx 4\%$ reduction from the AM-PSO perturbation method (0.00376). The c_{lmax} by the hybrid approach (1.7467) is compromised by $\approx 1\%$ from the AM-PSO method (1.7717), but is comparable to the baseline NLF(1)-0416 profile (1.75), with a percentage difference of $\approx 0.20\%$ considered negligible. The constraints relating to d_{cl}/d_x and c_{m0} are satisfied by the hybrid algorithm. Thus, the benefits of incorporating a coupled global-local search optimisation methodology, for drag minimisation is validated.

The feasibility of the design coefficients by the hybrid approach is verified by the perturbation method from Section 5.4. The data is clustered with priority to drag to determine if lower c_d solution regions exist about the hybrid optimal shape. The equating influence on c_{lmax} and aerofoil shape coefficients is presented in Fig. 8.

The lowest c_d performance by the perturbation process, matches the optimal magnitude by the hybrid approach ($c_d = 0.00362$). Thus, the solution is within a validated search topology. The drag contour magnitudes in Fig. 8(a) are restricted to the computed minimum drag performance. Thus, darker contour regions correspond to profiles with drag performances higher than the established optima. By restricting the drag contour magnitudes to low values, nine aerofoils with $c_d = 0.00362$, matching the hybrid shape are observed in the search topology (Fig. 8(a)). The shapes are comparable, with variations restricted to the nose radius curvature on the lower surface (Fig. 8(c)).

When the drag performance between aerofoils is the same, preference to shape with higher c_{lmax} subject to all design constraints satisfied, is set. The variation in c_{lmax} between the nine sections in Fig. 8(b), indicates the hybrid approach with the highest c_{lmax} is $\approx 0.50\%$ greater than the perturbation shape. The c_{lmax} decreases as the search topology shifts towards the top-right corner of the SOM in Fig. 8(b). The sample aerofoil is computed with the lowest c_{lmax} but the variation is restricted to $\approx 1\%$ less than the optimal shape. Thus, aerofoil shape design coefficients by the hybrid optimisation approach, are validated through the qualitative representation of the solution topology.

C. Multi-point design

The validation approach in single-point designs, is applied for multi-point analysis. Aerofoil performance by the AM-PSO, perturbation of the AM-PSO, hybrid-based optimisation and post-processing of the hybrid profile by independent variable manipulation, is presented in Table 10 and 11 at cruise and climb c_l^T of 0.40 and 1.00 respectively.

The hybrid optimisation approach yields lower c_d at $c_l^T = 0.40$ and $c_l^T = 1.00$ (Table 10-11), than the initial AM-PSO solution (Table 7-8). The design validation analysis indicates aerofoil shape variables by the AM-PSO methodology, did not converge to a global optima. The hybrid optimisation approach reduces drag by $\approx 7\%$ and $\approx 11\%$ at cruise and climb, in comparison to the solution by the AM-PSO method (Table 7-8). The c_{lmax} increased by $\approx 1.00\%$, with all constraints satisfied (Table 10). Further, validation of the perturbation solution to the hybrid profile, indicates no design improvement in c_d . The c_{lmax} by the perturbation approach is marginally greater (1.7738 vs 1.7605 in Table 10) than the hybrid shape optimisation profile, but at the expense of higher drag (0.00472 vs 0.00468 at $c_l^T = 0.40$ & 0.00604 vs 0.00590 at $c_l^T = 1.00$ in Table 11), at the two flight conditions examined.

Table 10
Multi-point results by AM-PSO, AM-PSO perturbation, hybrid optimisation and hybrid perturbation approach at $c_l^* = 0.40$

Method	t/c	Max Camber	c_l	AOA	c_d	% c_d Gain	c_{lmax} $R_n = 3 \times 10^6$	% c_{lmax} Gain	d_{cp}/d_x	C_{m0}
NLF(1)-0416	0.16	0.025	0.40	-0.695	0.00502	—	1.7500	—	0.2493	-0.0994
AM-PSO	0.175	0.027	0.40	-1.396	0.00464	-↓7.57	1.7440	-↓0.34	0.3056	-0.0901
AM-PSO Perturbation	0.166	0.028	0.40	-0.885	0.00466	-↓7.17	1.7725	+↑1.27	0.2913	-0.0902
Hybrid AM-PSO/GM	0.166	0.033	0.40	-2.220	0.00468	-↓6.77	1.7605	+↑0.60	0.295	-0.0984
Hybrid Perturbation	0.174	0.030	0.40	-2.270	0.00472	-↓5.97	1.7738	+↑1.34	0.2931	-0.0988

The variance of aerofoil shape variables r_{teup} , r_{telow} , y_{te} , t_{egup} , t_{eglow} , t_{ewup} , t_{ewlow} , x_w , y_w , y_{xw} , x_b between the hybrid optimisation and the equating perturbation approach is limited to $\approx <0.50\%$. Shape modification thus, performance differences between the final hybrid and perturbation solution is limited to $\approx 1\%$ for y_l and y_{xcl} (Fig. 9). The convergence of y_l and y_{xcl} by the AM-PSO, perturbation of the AM-PSO, hybrid AM-PSO / GM and the equating perturbation approach, is validated in Fig. 9.

Variable magnitude differences of y_l and y_{xcl} between the AM-PSO and the equating perturbation validation approach is significant. Relatively the variances between the AM-PSO/GM optimisation approach and the pre-processing validation process, is minimal (Fig. 9). Thus, it is concluded that the hybrid optimisation approach, has converged to a global solution for the DNO modules applied.

6.0 CONCLUSION AND FUTURE WORK

An intelligent shape optimisation architecture for HALE aerofoil shape design is developed and validated. The optimisation architecture is defined to facilitate efficient optimisation search simulations for solution feasibility. The following is a summary of findings:

- The gradient based method is sensitive to multimodal search topologies associated with aerofoil design problems and will generate a sub-optima solution. The search method yields a local solution to the starting point and not the true optima. To address the identified demerits, global search evolutions strategies are applied;
- A variant of the original PSO model is proposed with an adaptive-mutation operator. The method introduces mutation thus, search diversity in a time-iteration based process;
- The performance of the AM-PSO algorithm is assessed on several uni and multi-modal benchmark mathematical test functions. The results converge to the global optima with fewer design iterations in comparison to the best algorithm reported in the literature;
- The efficiency of the search process for aerofoil shape design, is enhanced by defining the search limits of the design variables. A novel, inverse shape fitting design study is developed;
- A sensitivity study is applied to determine the effect of shape variables on aerofoil aerodynamics hence, the objective function. The design variables are ranked in order of importance and the lowest ranked coefficient is identified and eliminated;
- Aerofoil shape optimisation with the developed AM-PSO model is initiated. The objective function minimises drag at specified c_l^* with the constraint on c_{lmax} , t/c , c_{m0} and d_{cp}/d_x . Convergence of solution search space is examined by varying aerofoil shape parameterisation type and design variable population size;
- The results of the single-point design optimisation indicated a global solution about the input c_l^* at cruise. Elsewhere drag is high thus, indicating the demerits of the single-point approach. The variant of the PARSEC method with thirteen variables indicated a $\approx 2\%$ reduction in drag compared to the original method with eleven variables;

- The effect of design variable elimination by the proposed pre-screening method, on objective function and iterations to convergence is established. A minimal effect on drag with significantly fewer iterations to convergence was established for single-point design optimisation;
- The results of the multi-point design are comparable to the baseline shape. Drag is significantly lower for the specified c_l^* range, than the theoretical validation aerofoil;
- The effect of design variable elimination for multi-point designs, increases drag slightly while significantly reducing the computational time to convergence. The aerodynamic performance deviations of the optimal solution by the full and reduced set of shape variables, is minimal; and
- A hybrid optimisation approach by the integration of a gradient based solver is introduced. The final solution by the AM-PSO method is applied for search initialisation to the GM solver. The true optimum is established with minimal drag performance, in comparison to a global based optimisation simulation. A novel technique with self-organising maps is applied to validate the optimality of the final solution. The qualitative approach confirms the scope of the search topology. Hence, the feasibility of the proposed solution is validated.

Future design studies will focus on:

- Increasing the sample size of the aerofoils examined in the inverse shape fitting process for solution space mapping;
- Verifying the convergence of the solution search space, by increasing the design variable population size. The CST method by Kulfan⁽⁴⁹⁾ will be applied;
- A robust shape optimisation process will be formulated to address the uncertainty of selecting flight point for optimisation in multi-point designs. A similar concept has been developed by Huyse^(50,51);
- A high-fidelity flow solver will be integrated into the DNO process to enhance viscous drag prediction; and
- The developed AM-PSO model will be integrated to a surrogate model in the form of neural networks⁽⁴³⁾ and Kriging^(8,52) to further reduce the computational time to convergence.

Table 11
Multi-point results by AM-PSO, AM-PSO perturbation, hybrid optimisation and hybrid perturbation approach at $c_l^* = 1.00$

Method	Max	c_l	AOA	c_d	% c_d Gain
NLF(1)-0416	0.025	1.00	4.479	0.00661	—
AM-PSO	0.027	1.00	3.677	0.00612	-↓7.41
AM-PSO Perturbation	0.028	1.00	4.187	0.00610	-↓7.72
Hybrid AM-PSO/GM	0.033	1.00	2.820	0.00590	-↓10.74
Hybrid Perturbation	0.030	1.00	2.763	0.00604	-↓8.62

ACKNOWLEDGMENTS

Dr Gerhard Kranner, Viscovery Software GmbH: For his technical assistance/discussions on the application of Viscovery SOMine 5.2, for shape optimisation applications;

Robert Carrese, RMIT PhD Research Candidate: For his technical assistance in evaluating the results of the design variable sensitivity analysis, and;

Victorian Partnership for Advanced Computing: For providing the supercomputing infrastructure and technical support to facilitate shape optimisation by parallel computing.

REFERENCES

- SOMERS, D.M. Subsonic aerofoil design. Website: Access Date 7th October 2009. <http://www.aerofoils.com/design.pdf>.
- HICKS, R.M. and HENNE, P.A. Wing design by numerical optimisation. *J Aircr*, 1977, **15**, pp 407–413.
- KEANE, A.J. and NAIR, P.B. *Computational Approaches for Aerospace Design: The Pursuit of Excellence*, John Wiley & Sons, West Sussex, England, UK, 2005.
- GALLART, M.S. Development of a Design Tool for Aerodynamic Shape Optimisation of Aerofoils. Master's thesis, Department of Mechanical Engineering, University of Victoria, Australia, 2002.
- VICINI, A. and QUAGLIARELLA, D. Inverse and direct aerofoil design using a multiobjective genetic algorithm. *AIAA J*, 1997, **35**, pp 1499–1505.
- TOPLISS, M.E., TOOMER, C.A. and HILLS, D.P. Aerodynamic optimisation using analytic descriptions of the design space, *J Aircr*, **35**, pp 882–890, 1998.
- PEIGIN, S. and EPSTEIN, B. Efficient approach for multipoint aerodynamic wing design of business jet aircraft. *AIAA J*, 2007, **45**, pp 2612–2621.
- D'ANGELO, S. and MINISCI, E.A. Multi-objective evolutionary optimisation of subsonic aerofoils by kriging approximation and evolutionary control. The 2005 IEEE Congress on Evolutionary Computation, **2**, pp 1262–1267, 2005.
- SOBIECZKY, H. Parametric aerofoils and wings, *Numerical Fluid Dynamics*, 1998, **68**, pp 71–88.
- CHAOUAT, B. Reynolds stress transport modelling for high-lift aerofoil flows, *AIAA J*, 2006, **44**, pp 2390–2402.
- HELLSTEN, A. New advanced k - ω turbulence model for high lift aerodynamics. *AIAA J*, 2005, **43**, pp 1857–1869.
- SCHOLZ, U., WINDTE, J. and RADESPIEL, R. Validation of the RANS-simulation of laminar separation bubbles on aerofoils, *Aerospace Science and Technology*, **10**, 2005, pp 484–494.
- CHOI, S. and KWON, O. Aerodynamic characteristics of elliptic aerofoils at high Reynolds numbers, *J Aircr*, 2008, **45**, pp 641–650.
- KERN, S. Evaluation of turbulence models for high-lift military aerofoil flowfields. In 34th Aerospace Sciences Meeting & Exhibit, Reno, NV, USA, 1996.
- NAMGOONG, H. Aerofoil Optimisation of Morphing Aircraft. PhD thesis, Aerospace Engineering, Purdue, Indiana, USA, 2005.
- NAKAHASHI, K., TAKAHASHI, S. and OBAYASHI, S. Inverse design optimization of transonic wings based on multi-objective genetic algorithms. *AIAA J*, **37**, pp 1656–1662, 1999.
- KHURANA, M., WINARTO, H. and SINHA, A. Aerofoil optimisation by swarm algorithm with mutation and artificial neural networks. In 47th AIAA Aerospace Sciences Meeting, Orlando, Florida, USA, 2009.
- GIANNAKOGLU, K.C. and PAPADIMITRIOU, D.I. *Adjoint Methods for Shape Optimisation*, **4**, pp 79–108, 2008, Springer-Verlag Berlin/Heidelberg.
- HOLLAND, J. *Adaption in Natural and Artificial Systems*. University of Michigan Press, Ann Arbor, Michigan, USA, 1974.
- GELATT, S., KIRKPATRICK, C.D. and VECCHI, M.P. *Optimisation by simulated annealing, Science. New Series*, 1983, **220**, pp 671–680.
- COLONI, A. and MANIEZZO, V. Distributed optimisation by ant colonies. In European Conference on Artificial Life, Paris, France, pp 134–142, 1991.
- KENNEDY, J. and EBERHART, R. Particle swarm optimisation. In IEEE International Conference on Neural Networks, Perth, Australia, pp 1942–1948, 1995.
- DRELA, M. and HAROLD, Y. XFOIL 6.9. <http://www.web.mit.edu/drela/Public/web/xfoil/>, last access on 18 February 2010.
- SHI, Y. and EBERHART, R. A modified particle swarm optimiser. In IEEE World Congress on Computational Intelligence, pp 69–73, 1998.
- EBERHART, R.C. and SHI, Y. Particle swarm optimisation: Developments, application, and resources. In IEEE Congress on Evolutionary Computation CEC2001, pp 81–86, 2001.
- HALGAMUGE, S.K., RATNAWEERA, A. and WATSON, H.C. Self-organising hierarchical particle swarm optimiser with time-varying acceleration coefficients. *IEEE Transactions on Evolutionary Computation*, 2004, **8**, pp 240–255.
- LUO, Q., CHEN, M.R. and LU, Y.Z. A novel hybrid algorithm with marriage of particle swarm optimisation and external optimisation. Technical report, Shanghai Jiaotong University, China.
- FU, J., WANG, L., WANG, X. and ZHEN, L. A novel probability binary particle swarm optimisation algorithm and its application, *J Software*, 2008, **3**, pp 28–35.
- QIN, A.K. and LIANG, J.J. Comprehensive learning particle swarm optimiser for global optimisation of multimodal functions, *IEEE Transactions on Evolutionary Computation*, 2006, **10**, pp 281–295.
- LAMBERT-TORRES, P.B., ALVARENGA, G.B. and ESMIN, A.A.A. Hybrid evolutionary algorithm based on PSO and GA mutation. In Proceedings of the Sixth International Conference on Hybrid Intelligent Systems HIS '06), Auckland, New Zealand, 2006.
- JANCIC, M., STACEY, A. and GRUNDY, I. Particle swarm optimisation with mutation. In *Evolutionary Computation*, Canberra, Australia, pp 1425–1430, 2003.
- HIGASHI, N. and IBA, H. Particle swarm optimization with Gaussian mutation. In Swarm Intelligence Symposium, Indianapolis, Indiana, USA, pp 72–79, 2003.
- SHI Z., QIN, YU, F. and WANG, Y. *Adaptive Inertia Weight Particle Swarm Optimization*, pp 450–459, Springer-Verlag Berlin/Heidelberg, 2006.
- SRINIVASAN, D. and SEOW, T.H. Particle swarm inspired evolutionary algorithm PS-EA) for multicriteria optimisation problems. In Proceedings of Evolutionary Computation, Canberra, Australia, pp 147–165, 2003.
- EBERHART, R.C. and SHI, Y. Fuzzy adaptive particle swarm optimization. In Proceedings of Evolutionary Computation, Seoul, Korea, pp 101–106, 2001.
- MA, L.H., ZHENG, Y.I. and QIAN, J.X. Empirical study of particle swarm optimizer with an increasing inertia weight. Technical report, Shanghai Jiaotong University, China, 2003.
- ZHENG, J., CUI, Z. and SUN, H. *Adaptive Velocity Threshold Particle Swarm Optimization*, pp 327–332. Springer-Berlin/Heidelberg, 2006.
- FANG, S.K.S. and CHANG, J.M. *A Modified Particle Swarm Optimiser Using an Adaptive Dynamic Weight Scheme*, pp 56–65. Springer-Berlin/Heidelberg, 2007.
- ROBINSON, J.J. and RAHMAT-SAMII, Y. Particle swarm optimisation in electromagnetics. *IEEE Transactions on Antennas and Propagation*, 2004, **52**, pp 397–407.
- WEI, J. and WANG, Y. A dynamical particle swarm algorithm with dimension mutation, *IJCSNS International J Computer Science and Network Security*, 2006, **6**, pp 221–224.
- RASMUSSEN, T.K., LOVBJERG, M. and KRINK, T. Hybrid particle swarm optimizer with breeding and subpopulations. In Proceedings of Genetic and Evolutionary Computing Conference, San Francisco, California, USA, pp 469–476, 2001.
- ZHANG, W.J., XIE, X.F. and YANG, Z.L. A dissipative particle swarm optimization. In Congress on Evolutionary Computation, Hawaii, USA, pp 1456–1461, 2002.
- KHURANA, M., WINARTO, H. and SINHA, A. Application of swarm approach and artificial neural networks for aerofoil shape optimization. In 12th AIAA/ISSMO Multidisciplinary Analysis and Optimisation, Victoria, British Columbia, Canada, 2008.
- MORRIS, M.D. Factorial sampling plans for preliminary computational experiments, *Technometrics*, 1991, **33**, pp 161–174.
- CAMPOLONGO, F., SALTELLI, A., TARANTOLA, S. and RATTO, M. *Sensitivity Analysis in Practice*. John Wiley and Sons, Ispra, Italy, 2004.
- CARBONI, J., CAMPOLONGO, F. and SALTELLI, A. An effective screening design for sensitivity analysis of large models, *Environmental Modelling & Software*, 2007, **22**, pp 1509–1518.
- KOHONEN, T. *Self-Organising Maps*. Springer, Berlin, Germany, 1995.
- Viscovery. Viscovery SOMine 5.1. <http://www.viscovery.net>, last access on 18 February 2010.
- KULFAN, B.M. and BUSSOLETTI, J.E. Fundamental parametric geometry representations for aircraft component shapes. In 11th AIAA/ISSMO Multidisciplinary Analysis and Optimization Conference, Portsmouth, Virginia, USA, 2006.
- HUYSE, L. and LEWIS, R.M. Aerodynamic shape optimization of two-dimensional aerofoils under uncertain conditions. Technical report, NASA Langley Research Center, 2001.
- LEWIS, R.M., HUYSE, L., PADULA, S.L. and LI, W. Probabilistic approach to free-form aerofoil shape optimization under uncertainty.
- MURAYAMA, M., JEONG, S. and YAMAMOTO, K. Efficient optimization design method using kriging model. In AIAA Aerospace Sciences Meeting and Exhibit, Reno, NV, USA.